Universidad Zaragoza
1542

Master Thesis

MEASUREMENT AND SIMULATION OF HOUSING SHIELDING PERFORMANCE

SEIBERSDORF LABORATORIES

Author

David Lorien Ara Sanz

Director

Stefan Cecil

Rapporteur

Francisco Manuel Lera García

School of Engineering and Architecture

December 2018

To Seibersdorf Laboratories, in particular to Stefan Cecil and the colleagues of the Electromagnetic Compatibility department for giving me this opportunity.

To Francisco Lera for helping me during the correction and presentation of this report.

Por último, a mi familia y amigos por el apoyo recibido durante todos estos años de estudio que concluyen con este proyecto.

Resumen

El Trabajo Fin de Máster que se presenta ha sido desarrollado en colaboración con la empresa Seibersdorf Laboratories (Viena, Austria), concretamente con el departamento de compatibilidad electromagnética. Una línea de investigación recientemente iniciada en la compañía está orientada al diseño de carcasas para la protección electromagnética de dispositivos eléctricos. Surge como respuesta a la necesidad de aislar los equipos para evitar tanto que el funcionamiento de estos se vea comprometido por agentes externos como que sean ellos mismos el origen de las interferencias. Introducirlos dentro de una caja metálica podría parecer la solución idónea, sin embargo, no es realista. A menudo es necesario establecer conexiones eléctricas con el exterior, puertas de acceso, ventilación... Por tanto, es fundamental definir un sistema de medida que permita evaluar el impacto que estas aperturas tienen sobre el apantallamiento electromagnético. Las fases de diseño y evaluación de estas estructuras en el laboratorio son lentas y complejas. Una buena solución para acelerar el proceso es el desarrollo de simulaciones capaces de modelar con precisión estos sistemas.

Bajo estas premisas, se inició en Seibersdorf Laboratories un primer proyecto enfocado en la medida y simulación del apantallamiento electromagnético ofrecido por una serie de láminas metálicas perforadas con distintos patrones. Estas placas fueron proporcionadas por la compañía Fronius, interesada en evaluar sus prestaciones electromagnéticas. La metodología de medida propuesta consistía en situar una antena receptora dentro de una cámara semi anecoica y otra transmisora fuera, ambas alineadas respecto a una apertura cuadrada situada en uno de los laterales de la cámara. El apantallamiento electromagnético ofrecido por las láminas se definió como la atenuación en la potencia recibida cuando estas eran situadas en la apertura de la cámara. Las medidas se realizaron con antenas *Bilog* y *Horn* en los rangos [30 MHz – 1GHz] y [1 GHz – 6 GHz] respectivamente. Además, el sistema de medida fue simulado con SEMCAD X. Estas primeras mediciones/simulaciones tuvieron en cuenta un reducido número de muestras y no se profundizó en la correcta configuración del sistema de medida. A su vez, los resultados mostraron importantes desviaciones entre medidas y simulaciones en el rango [30 MHz – 200 MHz].

Partiendo de la investigación mencionada y trabajando con 10 nuevas láminas (proporcionadas también por Fronius), se han realizado nuevas medidas y simulaciones que constituyen este Trabajo Fin de Máster. Para ello se han seguido los siguientes pasos:

- Ampliar el rango en el que se mide/simula el apantallamiento electromagnético incluyendo la banda [1 MHz – 30 MHz]. En este rango frecuencial se han usado antenas tipo *Loop* de acuerdo con el estándar IEEE 299.
- Estudiar la mejor configuración posible del sistema de medición, aquella que ofrezca un mayor rango dinámico en las medidas. Para ello se ha estudiado tanto la influencia de la distancia entre antena y lámina como el uso de otras antenas no consideradas previamente (*Biconical* y *LPDA*).
- Medir el apantallamiento de las 10 láminas y estudiar el impacto de realizar distintas modificaciones en las aperturas (forma, tamaño, material o el uso de pequeñas abrazaderas metálicas).
- Elaborar modelos adecuados de las 10 láminas que conduzcan a simulaciones precisas. Prestando especial interés al modelado de las abrazaderas (equivalen a conductores eléctricos perfectos) y la malla (modelada usando TRS y alta conductividad).
- Solucionar las divergencias entre medidas y simulación para la antena *Bilog* en el rango [30 MHz – 200 MHz]. Este desajuste es consecuencia de una excesiva diferencia entre los límites de la banda simulada (la máxima frecuencia (1 GHz) es 33 veces la mínima (30 MHz)).

El trabajo realizado ha conseguido mejorar el rango dinámico del sistema de medida e incrementar el ancho de banda analizado. A su vez, se tiene un mayor conocimiento del impacto sobre el apantallamiento electromagnético de distintos factores. Respecto a las simulaciones, su fiabilidad ha sido verificada frente a un mayor número de láminas, incluyendo además aperturas más complejas.

Al margen de los objetivos principales de este trabajo, se realizaron medidas del apantallamiento ofrecido por tres bloques de “piedra” y una malla metálica a petición de un cliente. Estos resultados quedan recogidos en los anexos B y C del informe.

Summary

This Master's Thesis has been developed in collaboration with Seibersdorf Laboratories (Vienna, Austria), specifically with the department of electromagnetic compatibility. A line of research recently started in the laboratories is focused on designing housings for the electromagnetic shielding of electronic devices. Isolating the equipment is essential for two reasons: prevent malfunctioning due to radiations coming from of other electronic systems and avoid being the source of the interferences. Placing the devices inside a metal box may seem like the ideal solution, however, it is not realistic. It is usually necessary electrical connections with the outside, access doors, ventilation ... Therefore, defining a measuring method to evaluate the impact that these apertures have on the electromagnetic shielding is fundamental to make optimal housings. However, the design of the structure and performance evaluation in the laboratory is highly complex and time-consuming. A good solution to accelerate the process is the development of precise simulations capable of modelling complex systems.

Under these premises, a first project initiated in Seibersdorf Laboratories focused on the measurement and simulation of the electromagnetic shielding performance offered by thin metallic sheets perforated with different patterns. These plates were provided by the Fronius Company, interested in evaluating its electromagnetic performance. The proposed set-up for the shielding determination consists in placing an antenna inside the semi-anechoic chamber and the other outside, both facing the square aperture in the wall of the chamber. The determined shielding in dB is the difference between the received power with opened set-up and with plate in the fixture. Bilog and Horn antennas were used in the ranges [30 MHz - 1 GHz] and [1 GHz - 6 GHz] respectively. In addition, simulations of the set-up were developed with SEMCAD X. These first measurements/simulations considered just a small number of sheets and did not study the optimal configuration of the set-up. Additionally, the results showed important deviations between measurements and simulations in the range [30 MHz - 200 MHz].

Using the mentioned research as a basis and 10 new plates (also provided by Fronius), we have continued developing this methodology, both laboratory measurements and simulations. For this, the following steps have been carried out:

- Expand the range in which the shielding is evaluated by adding the frequency range [1 MHz - 30 MHz]. In this new band Loop antennas have been used according to the IEEE 299 standard.

- Find the set-up configuration that offers the maximum SE measurable. For this purpose, the effect of the distance between the antenna and the sheet and the use of new types of antennas (Biconical and LPDA) has been studied.
- Measure the shielding effectiveness of the 10 sheets and study the impact of making different modifications in the openings (shape, size, material or using small clamps).
- Elaborate adequate models of the 10 plates in order to execute precise simulations. Special attention was paid modelling the clamps (equivalent to perfect electric conductors) and the net (modelled using TRS and assuming high conductivity).
- Fix the divergences between measurements and simulations with the Bilog antenna in the range [30 MHz - 200 MHz]. The origin is an excessive difference between the limits of the simulated bandwidth (the maximum frequency (1 GHz) is 33 times the minimum (30 MHz)).

By carrying out these steps the dynamic range of the measurements has been improved and the bandwidth analysed increased. At the same time, there is a greater knowledge of the impact on the shielding effectiveness of diverse factors.

Regarding the simulations, its reliability has been verified with a greater number of sheets, including more complex openings.

Apart from the main objectives of this project, measurements of the electromagnetic attenuation offered by three blocks of "stone" and a net were made at a client request. These measurements have been included in the annexes B and C of this report.

Table of Contents

List of Figures

List of Tables

List of acronyms

EMC	Electromagnetic Compatibility
SE	Shielding Effectiveness
FDTD	Finite-Difference Time-Domain
NA	Network Analyzer
EM	Electromagnetic
LPDA	Log-Periodic Dipole Array
DR	Dynamic Range
RAM	Radiation Absorbent Material
PEC	Perfect Electric Conductor
PMC	Perfect Magnetic Conductor
TRS	Thin Resistive Sheet

Chapter 1

Introduction

This first section is used as an introduction to the Master Thesis carried out. First, the context in which it has been developed and the objectives of the project will be established. Subsequently, the state of art and motivations will be explained, as well as the working methodology. Finally, the chapter concludes presenting the general structure of the report.

1.1 Context And Objectives

This project is the continuation of a previous investigation developed by the organization Seibersdorf Laboratories, specifically the department of Electromagnetic Compatibility (EMC), in collaboration with TU Graz and the company Fronius.

Seibersdorf Laboratories' offices are located 25 minutes far from Vienna, Austria, in a research centre shared with other institutions as the Austrian Institute of Technology (AIT) or the International Atomic Energy Agency (IAEA). It occupies 140 employees and is public property. The company offers "high-quality laboratories and analysis services as well as solution-driven Research & Development" in diverse fields: "International Training Programme", "Ionizing, Radiation and Radioactivity", "Pharmaceuticals", "Chemical Analytics", "Radiofrequency Engineering", "Laser, LED & Lamp Safety" and "Electromagnetic Compatibility".

The EMC department has more than 25 years of experience in "conformity evaluation of electronic devices and systems" to accomplish the European Union legal requirements. "By bundling the latest developments in measurement techniques up to the implementation of certified analytical procedures in one centre of excellence" Seibersdorf laboratories offers the customers a one-stop solution [1].

The interest in developing new measurement techniques is the cornerstone of this investigation, specifically for this project the evaluation of the impact produced by different slots and materials on the electromagnetic shielding effectiveness (SE) performance. This thesis pretends to enhance the existing SE measurement methodology by modifying diverse parameters (antennas, receiver, distances, ...) and develop suitable simulation models. The final goal is the creation of an accurate method appropriate for measurement and simulation of simple housing.

1.2 Motivation And State Of Art

Nowadays electronic devices have a fundamental function in modern societies, its wide application is a consequence of the cost reduction and performance improvement. New systems operate at higher speed requiring lower dimensions and, therefore, decreasing the distance between circuits. Special applications also demand high reliability, such as military equipment.

Under these conditions, EMC has become lately a topic of main importance to guarantee the correct operation of all these systems under diverse circumstances. The equipment should be immune to external noise/interferences and, at the same time, should not be a source of electromagnetic pollution [2].

A simple analysis of EMC troubles shows that the problem can be faced in 3 different ways [3]:

I. Suppress the noise/interference at its source. Sometimes it is not possible, for example when the interference is natural (solar flares, auroras, thunders, ...).

II. Make the coupling path (wireless or wired) as inefficient as possible.

III. Make the receptor less susceptible to the noise/interference.

This project focuses on the second solution, specifically, the design of housing for power electronic systems against wireless transmissions. Designing an efficient shielding can be very complex and time-consuming, to enhance the development of this technology new measurement and simulation methods must be applied.

First of all, a method to measure the attenuation obtained by using a certain shielding must be defined. A well-known starting point in this field is the standard IEEE 299, applicable in the frequency range [9 kHz – 19 GHz] (extendable to [50 Hz – 100 GHz]). Although this document is only valid for enclosures with dimensions greater than 2 m, it can be used as a reference for the set-up configuration (antennas, distances, ...). This standard is currently under development to extend its functionality to smaller enclosure size. Up to now, no standard has been widely accepted for physically small enclosures [4].

Last publications of the IEEE 299 Working Group [5], in charge of this investigation, suggests using a frequency-stirred reverberation chamber. It overcomes the two main problems of small enclosures: strong internal resonances and difficulty/impossibility to move the inside probe. Another advantage in comparison to plane wave methods is that the shielding is exposed to fields with diverse incidence directions and polarizations. This way the average SE can be measured for physically small but electrically large cavities. Jan Carlsson, Kristian Karlsson

and Andreas Johansson proved that the measured SE with this method fits the aperture theory [6].

In a different line of work, but with the same objective, M. Hromádka and Z. Kubík published a paper named "Suggestion for Changes in Shielding Effectiveness Measuring methods" proposing a system (Figure 1) that substitutes the reverberation chamber by an anechoic chamber [7].

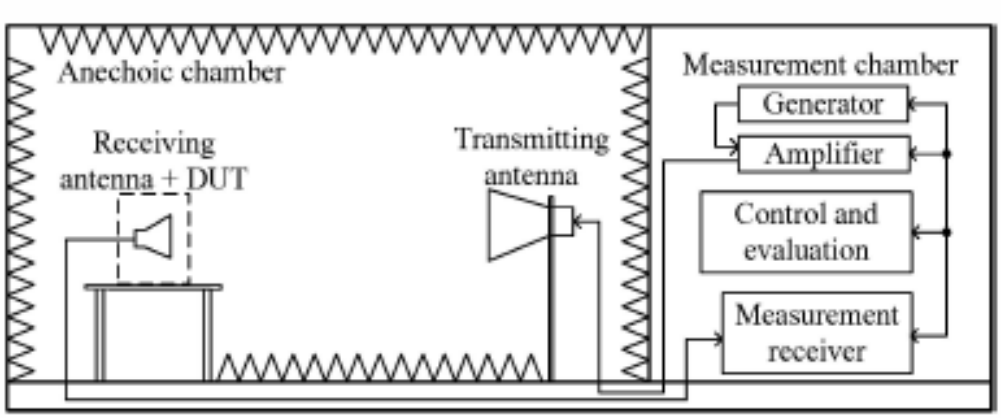

Figure 1 Measurement chain of shielding effectiveness [7]

All these previous investigations can be used as a reference to define the measuring method of this project. However, the specific requirements of the samples analysed, plane sheets and not enclosures, require a different approach (Chapter 4).

As important as the measurements for this project is the electromagnetic simulation of the set-up. Diverse numerical solutions can be used with this purpose: finite element method (FEM), finite-difference time-domain (FDTD) or method of moments (MoM) among others. The accuracy of these simulations has been proved in several investigations. An example is the good results obtained simulating the set-up in Figure 1 with COMSOL Multiphysics (FEM) (Figure 2) [8]:

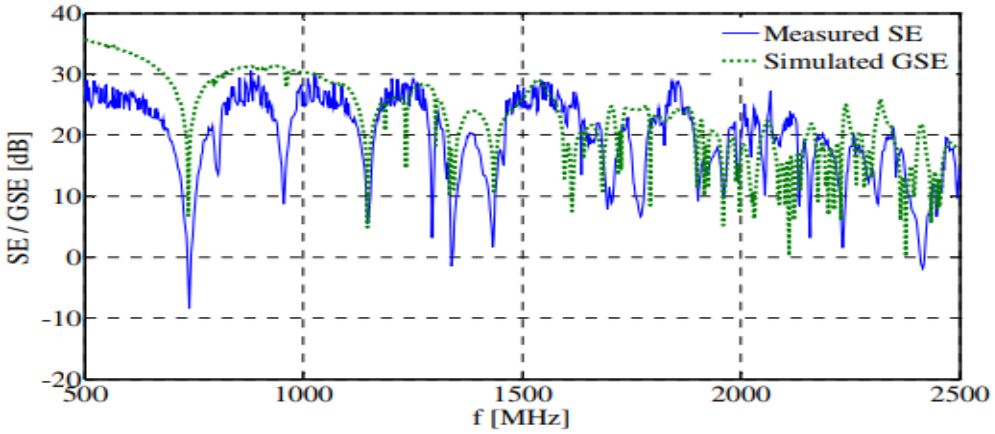

Figure 2 Comparison of results between measured SE and simulated GSE (Global SE) of 3D model [8]

Seibersdorf Laboratories has also previous experience in SE measuring/simulation, but with a different perspective. Earlier research in the company used metallic sheets integrated into a 315x315 mm square aperture of the anechoic chamber, rather than enclosures. This project studied the adequate correlation between simulations and measurements results in the range [30MHz – 6GHz] using two antennas (Bilog under 1GHz and Horn over 1GHz) and just a few plates with simple openings. SEMCAD X, a software based on the FDTD method, was used to execute the simulations.

The results of the research showed important divergences between simulations and measurements for frequencies under 300MHz. Furthermore, the previous study did not analyse the effect of modifying diverse parameters: distance antenna-wall, simulations broadband limit, use other antennas and study a larger variety of shielding openings. This previous knowledge is used as a starting point for the thesis.

1.3 METHODOLOGY

To achieve all the objectives of this project the following steps have been taken:

1. Theoretical analysis of electromagnetic compatibility, SE and state of the art.
2. Familiarization with the software SEMCAD X: modelling tools, electromagnetic simulation theory and simulations configuration.
3. Verification of the models already designed: Bilog antenna, Horn antenna and semi-anechoic chamber.
4. Modelling of the 10 plates evaluated.
5. Modelling of the Loop Antenna.
6. Configuration of the simulation parameters: voxels size, centre frequency, bandwidth, number of periods...
7. Execution of the numerical simulations using a high-speed performance solver.
8. Set up of the equipment and measurement.
9. Analysis of the results: comparison between measurement and simulations.
10. Proposition of solutions for those results in which measurement and simulation do not coincide.
11. Additional tests out of this project scope were conducted following a customer´s request, measuring the SE of three stones and a net. Results in Annex B and Annex C. No simulations were required by the client.
12. Elaboration of the report.

1.4 Report Structure

The report, in addition to this introduction, consists of 6 chapters and 3 annexes:

- **Chapter 2 Theoretical Analysis:** This chapter introduces the concept of SE from different points of view: theoretical, mathematical and its application to this project.
- **Chapter 3 Measurements Equipment:** This chapter presents the equipment necessary to do the SE measurements.
- **Chapter 4 Measurements of the Shielding Effectiveness:** This chapter starts outlining the configuration of antennas, semi-anechoic chamber, network analyzer (NA) and signal generator necessary to measure the SE. Subsequently, an analysis of the system is carried to identify the best setup configuration; selection of antennas and distances.
- **Chapter 5 Numerical Simulation – SEMCAD X:** This chapter introduces the simulation software/hardware used and the theoretical background on which it is based. Subsequently, the steps required to develop the simulations are explained: modelling, solver selection and configuration of the frequential parameters.
- **Chapter 6 Evaluation and Improvement of the Results:** This chapter presents and analyses the results obtained for each plate. The objective is the verification of the correct concordance between measurements and simulations. It is also important to detect the effect of other factors in the SE: electromagnetic (EM) clamps, aperture size/shape and material. In case of divergence, the cause is investigated to find a plausible solution.
- **Chapter 7 Conclusions and Future Research Lines:** This chapter offers a critical analysis of the results obtained during the investigation and proposes future lines of investigation.
- **Annex A Dimensions of the Plates Apertures:** This Annex contains a table that summarize the maximum opening size for each dimension and plate.
- **Annex B Stones Measurements:** This Annex contains the SE measures of three stones made of the same material but with different thicknesses (5, 10 and 15 cm.). The SE was measured in two different ways: with the methodology used for this project and inside a fully-anechoic chamber.
- **Annex C Net Measurements:** This Annex contains the SE measurements of a metallic net. It has been added to the report in order to include all the tests done in the anechoic chamber, but it is not part of the thesis objectives.

Chapter 2

Shielding Effectiveness Analysis

This chapter introduces the concept of SE from different points of view: theoretical, mathematical and its application to this project.

2.1 Theoretical Concept

The term shielding effectiveness reflects the capability of a structure to attenuate electromagnetic fields, it consists in the addition of the absorption loss, reflection loss and re-reflection correction factor [9]. The final value is influenced by several factors:

- Material of the shielding.
- Size and shape of the shielding and its openings.
- Frequency of the wave.
- Distance from the source to the shielding: far-field or near-field region.
- In case of the near-field; type of predominant field component: electric or magnetic.
- Angle of incidence of the wave.

According to these factors, the complete electromagnetic shielding performance of the structure cannot be defined with one single value and is conditioned to the incident field characteristics.

2.2 Mathematical Concept

The most common definition of SE, represented in Figure 3, stablish a ratio between the incident and the transmitted electric/magnetic component.

$$S_E(f)[dB] = 20\log_{10}\left(\frac{E_i(f)}{E_t(f)}\right) \qquad \textit{Equation 1}$$

$$S_H(f)[dB] = 20\log_{10}\left(\frac{H_i(f)}{H_t(f)}\right) \qquad \textit{Equation 2}$$

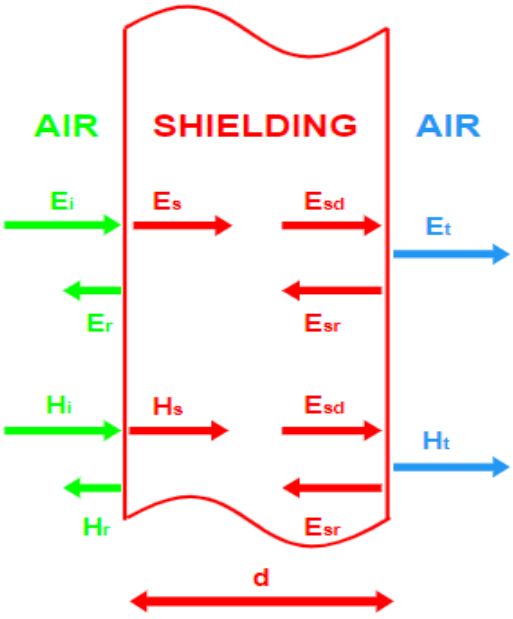

Figure 3 Schematic of the shielding effect

This formulation assumes an infinite sheet that eliminates the edging effect. On that basis, several equations have been developed to estimate the SE for simple openings or homogeneous materials [10].

However, this definition has unfeasible requirements in the laboratory:

I. Infinite sheet.

II. Plane-Wave.

III. Measuring incident and transmitted field in the proximity of the shielding.

Therefore, SE must be redefined in a more practical way:

$$SE(f)[dB] = 10\log_{10}\left(\frac{Power\ received\ without\ shielding(f)}{Power\ received\ with\ shielding(f)}\right) \qquad \textit{Equation 3}$$

The ratio between the power received by the antenna in two different scenarios gives a wide range of possible configurations: antennas, distances, reference scenario, electromagnetic wave characteristics, …

2.3 Practical Application

Once a feasible formulation of the SE has been selected, its application to a real measuring method must be analysed. The set-up configuration is constrained by the objectives of the project and the equipment available.

I. This project analyses the shielding performance of 10 drilled sheets, and not the shielding of a specific electronic device or enclosure.

II. The size of the plates is limited, its equivalence to infinite large sheets cannot be assumed. The leakage through the borders of the plate (Edging effect) is too important, it would distort the effect of the plate opening. It restricts the selection of the reference scenario (without shielding).

Following these premises Seibersdorf Laboratories has developed a method for the shielding determination in the semi-anechoic chamber. The set-up consists out of plates integrated in the square opening of the chamber and two identical antennas (one inside and another outside of the chamber) (Figure 4).

Figure 4 Set-up for the SE determination with the LPDA antenna

The determined SE in dB is the difference between the received power with opened set-up and a plate in the fixture. Standard IEEE 299 suggests, if the noise level is low enough, running all the test with the transmitting antenna inside and the receiver outside. Nevertheless, we decided to place the transmitter outside to work with the least possible noise level at the receiver side.

Earlier projects had worked in the frequency range [30 MHz – 6 GHz] with the Bilog and Horn antennas, this thesis pretends to include other types: Biconical and Log-Periodic Dipole Array (LPDA). It is in line with the IEEE 299 standard: "in the resonance range (20 MHz to 300 MHz), biconical and electric dipoles are recommended; and in the high range (300 MHz to 18 GHz) dipoles, horns, or equivalent antennas can be used.".

These antennas are placed aligned to the centre of the square opening and the distance antenna-wall (equal for both) is defined using the plate as a reference (Figure 5). The SE measured with these antennas is related to the electric field attenuation.

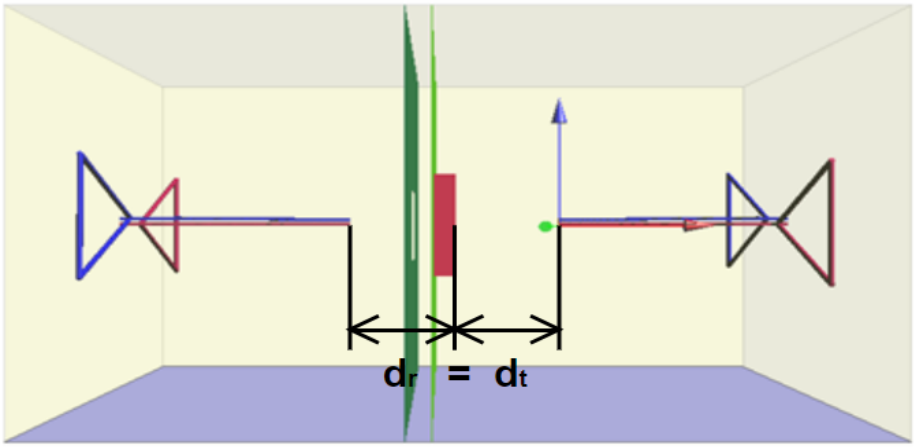

Figure 5 Model of the set-up for the SE determination with the Bilog antenna

Another objective of this project is to study the SE at lower frequencies, 1 MHz to 30 MHz. IEEE 299 does not provide a procedure to measure the electric-field SE in this range because the experience shows that "the most stringent requirement involves the effectiveness of magnetic-field shielding" [4]. The method proposed by the standard consists in the use of two small electrostatically shielded loops (diameter smaller than 1 m) to evaluate the attenuation of the opening against magnetic fields.

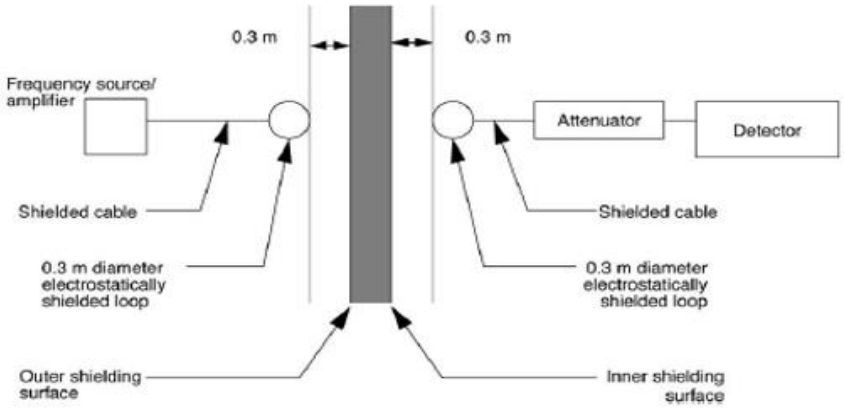

Figure 6 IEEE 299: Schematic diagram of the test configuration for magnetic test showing dimensions of transmit and receive antennas (coplanar antenna orientations) [8]

As can be seen in Figure 6, the antenna-wall distance is set by the standard in function of the inner/outer shielding surface (the total distance between antennas depends on the wall width). For the previous antennas, the reference had been set in relation to the plate, so the results could be compared to earlier investigations. In this case, there are no preceding results for the Loop antenna and the definition of antenna-wall distance can be modified to fit the IEEE 299 standard (Figure 7).

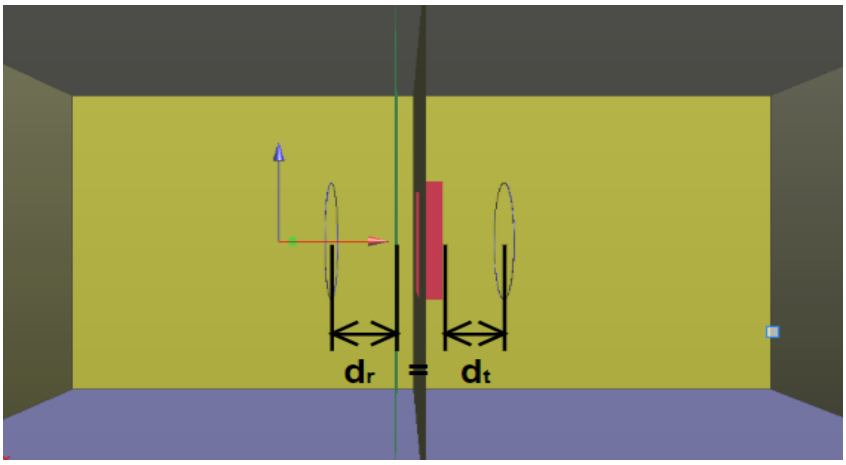

Figure 7 Model of the set-up for the SE determination with the Loop antenna

Another relevant factor that must be considered is the maximum SE measurable. This limitation can be consequence of: equipment, noise or leakage through the connections between the plate and the wall. Stablishing this limit is fundamental to know the dynamic range (DR) within we can have confidence in the results. According to the IEEE 299 standard, SE shall be at least 6 dB lower than the DR to be a valid measure.

DR definition of the IEEE 299: difference between the reference level and the minimum discernible signal above the noise floor. The minimum discernible signal is defined as one with an amplitude of 3 dB or more above the test system noise floor.

However, this definition is not appropriate for the set-up of this project. Meanwhile the standard is elaborated for enclosures, this investigation is using the integration of plates in the chamber opening. It means that the leakage through the connections between both parts is going to be a limitation that the standard does not deal with. Hence, the DR must be redefined.

DR definition for this project: difference between the power received with a plate without openings and opened set-up (Figure 8). This way, the DR establishes the maximum SE measurable equal to the point where the leakage through the borders is more relevant than the plate aperture.

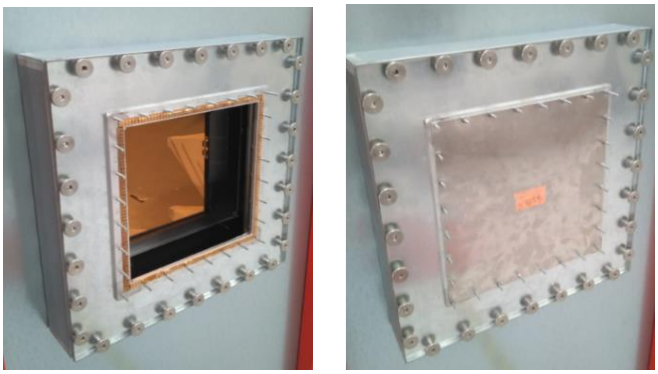

Figure 8 Opened (Left) and Closed (Right) configuration

2.4 SLOT ANTENNA THEORY

When the wavelength is comparable to the openings size the "intrinsic shielding effectiveness of the shield material is of less concern than leakage through the apertures". At these frequencies, applying the slot antenna theory is a useful approach in order to understand the dependency between SE and frequency.

The "slot antenna is a most efficient radiator when its maximum linear dimension", perpendicular to the electric field, "is equal to ½ wavelength" (Figure 9). For shielding applications implies that the lowest SE should appear at this frequency (Equation 4) [2].

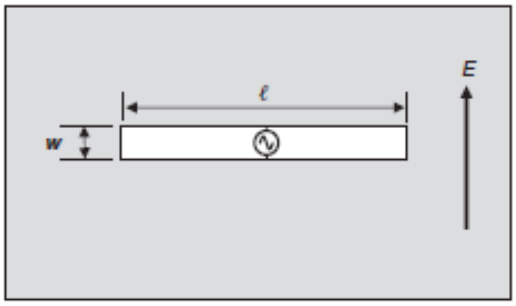

Figure 9 Slot Antenna [2]

$$f = \frac{c}{\lambda} = \frac{c}{2 \cdot L} \qquad \textit{Equation 4}$$

Chapter 3

Measurements Equipment

In this passage the equipment necessary for the measurements is presented. First, the concept and characteristics of the semi-anechoic chamber is explained. Subsequently, the plates analysed are shown and briefly commented. Transmitter and receiver are introduced as well, and its selection among other options is justified. The chapter concludes presenting the different available antennas and its principal characteristics.

3.1 Semi-Anechoic Chamber

The term anechoic chamber is used to describe a room designed to approximate electromagnetic/acoustic free space conditions indoor. This investigation, obviously, requires a chamber designed for electromagnetic waves (Figure 10 and Figure 11). It ideally implies two main characteristics:

I. The interior is isolated from waves originated in the outside.

II. The walls of the room absorb any incident wave, there is no reflection. Radiation absorbent material (RAM) covers all the surfaces. When the floor is not protected with absorbent material, as in this case, the space is called semi-anechoic.

Figure 10 Inside of the Semi-Anechoic chamber

Figure 11 Outside of the Semi-Anechoic chamber

This chamber is used completely closed during normal test procedures at Seibersdorf Laboratories. However, the specific requirements of this investigation demand the use of the lateral aperture (highlighted in Figure 11) located to the right of the entrance door.

3.2 PLATES

The 10 plates under analysis have been provided by the company Fronius to evaluate the influence on SE of its shape, material and clamps. All of them have in common the dimensions (360x360 mm) and the drilled holes near to the borders that allow the proper connection to the semi-anechoic chamber.

According to the characteristic of each plate, four main groups can be established:

I. Plates Nº1-5: All these plates have been drilled with diverse 2-dimensional shapes (Example in Figure 12).

II. Plates Nº6-8: 18 circular holes drilled on a row. The difference is the diameter (6/7: 4.5mm, 8: 3 mm.) and the material (6/8: completely aluminium, 7: one half aluminium and the other an unknown metallic material, Fronius did not provide this information) (Example in Figure 13).

III. Plate Nº9: This is a special case; the structure can be modified to vary the width of the aperture. Also, two different types of clamps (Length: 1.2 and 2 cm) can be added to connect both sides of the opening (Example in Figure 14).

IV. Plate Nº10: It is a 3-dimensional structure composed of two materials: aluminium (as well as the others) and a metallic net of unknown properties (Example in Figure 15).

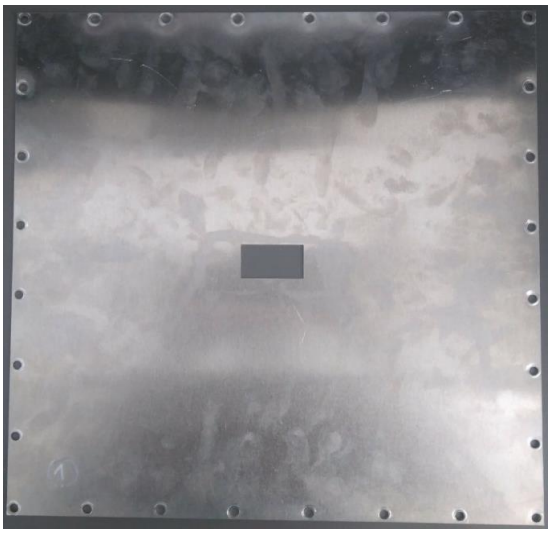

Figure 12 Image of Plate Nº1 (Group 1)

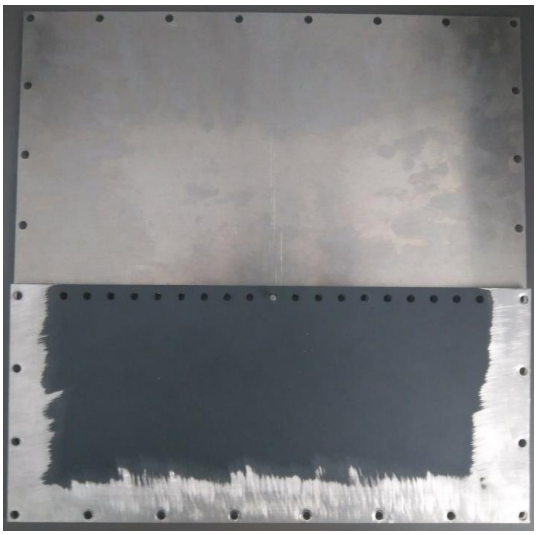

Figure 13 Image of Plate Nº7 (Group 2)

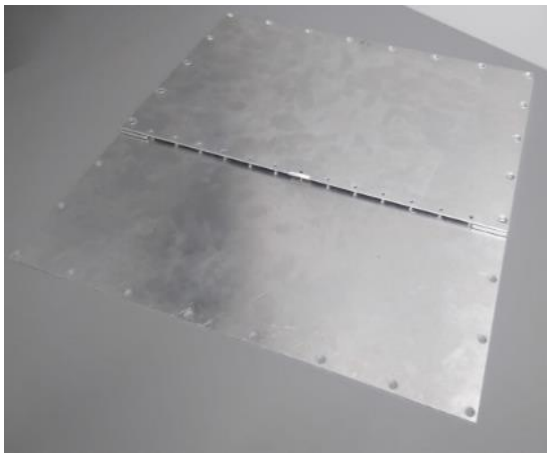

Figure 14 Image of Plate Nº9 (Group 3)

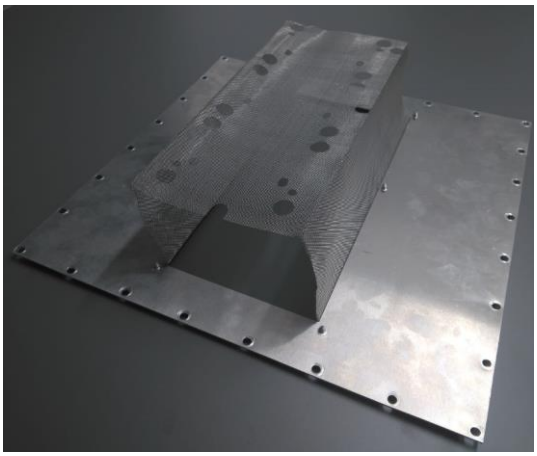

Figure 15 Image of Plate Nº10 (Group 4)

The clamps mentioned previously are shown in Figure 16:

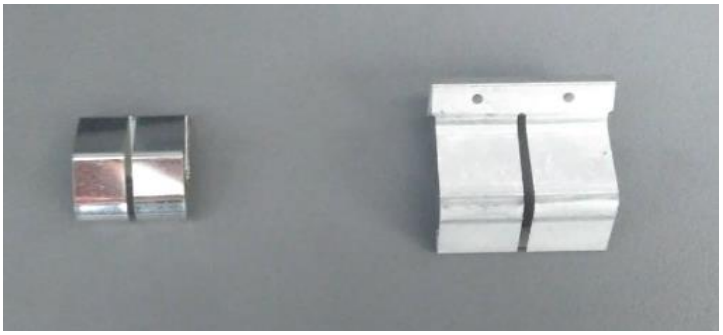

Figure 16 Image of the Clamps (1.2 cm - Left, 2 cm - Right)

3.3 Network Analyzer And Signal Generator

The electronic equipment in charge of transmitting and receiving the signal was chosen with one main requirement: fully cover the bandwidth analysed to simplify the measurements.

	Signal Generator	**Network Analyzer**
Manufacturer	Rohde & Schwarz	Rohde & Schwarz
Model	SMB100A	ESW-8
Frequency range	100 kHz to 40 GHz	2 Hz to 8 GHz
Max. Output Power	Over 16 dBm	-
Measurement Uncertainty	-	± 0.37 dB
Image of the device		

Table 1 Signal Generator [11] and Network Analyzer [12] Characteristics

3.4 Antennas

To cover all the frequencies under analysis, [1MHz – 6GHz], four distinct types of antennas are necessary. Its main properties will be presented below. The selection of each antenna is based on the frequency range that must be covered and its availability in the laboratory.

3.4.1 Loop Antenna

For the lowest frequencies the loop antenna will be the one used. Unlike the others, the magnetic field is the predominant component for this antenna in the near field. This difference must be considered during the analysis of the SE results [13].

Model	HLA 6121
Frequency Range	9 kHz – 30 MHz
Diameter (mm)	600
Weight (Kg)	2

Table 2 Characteristics of HLA 6121

Figure 17 HLA 6121: Schematic (Left), Transmitter (Middle) and Receiver (Right)

3.4.2 Biconical Antenna

The use of this antenna was not planned, and it is consequence of the deficient performance offered by the "Bilog" antenna in the range [30-100] MHz. This setback will be explained in future sections [14].

Model	VBA 6106A
Frequency Range	30 MHz – 300 MHz
Dimensions (mm)	1360 x 770 x 515
Weight (Kg)	1.3

Table 3 Characteristics of VBA 6106A

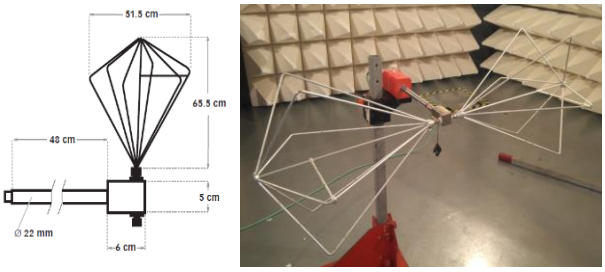

Figure 18 VBA 6106A: Schematic (Left) and Image (Right)

3.4.3 LPDA Antenna [15]

Model	UPA 6109
Frequency Range	200 MHz – 1 GHz
Dimensions (mm)	1000 x 750
Weight (Kg)	1.5

Table 4 Characteristics of UPA 6109

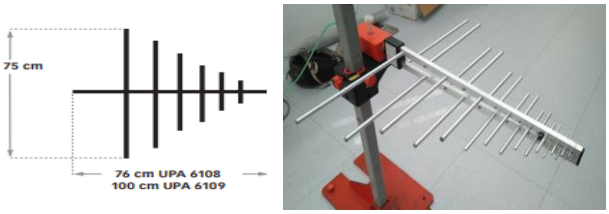

Figure 19 UPA 6109: Schematic (Left) and Image (Right)

3.4.4 Bilog Antenna

The "Bilog" antenna is a mixture between the two previous types: Biconical and Logarithmic. It is a way to increase the bandwidth of the LPDA by introducing a resonant section for lower frequencies. Two different models of "Bilog" antenna are present in the laboratory and can be used to cover the range [30 MHz – 1GHz], its performance is practically the same and have been used indifferently depending on its availability [16, 17].

Model	CBL 6111D
Frequency Range	30 MHz – 1 GHz
Dimensions (mm)	1310 x 1390 x 630
Weight (Kg)	3.5

Table 5 Characteristics of the CBL 6111D

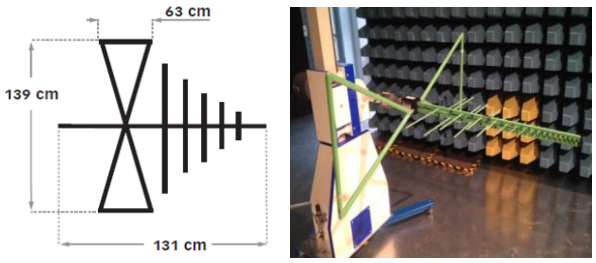

Figure 20 CBL 6111D: Schematic (Left) and Image (Right)

Model	CBL 6143A
Frequency Range	30 MHz – 3 GHz
Dimensions (mm)	1525 x 980 x 410
Weight (Kg)	4.2

Table 6 Characteristics of CBL 6143A

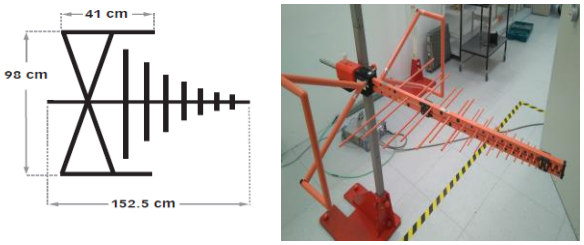

Figure 21 CBL 6143A: Schematic (Left) and Image (Right)

3.4.5 Horn Antenna [18]

Model	BHA 9118
Frequency Range	1 GHz – 18 GHz
Dimensions (mm)	240 x 147 x 247
Weight (Kg)	1.9

Table 7 Characteristics of BHA 9118

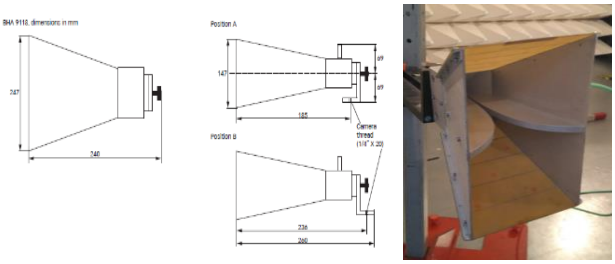

Figure 22 BHA 9118: Schematic (Left) and Image (Right)

Chapter 4

Measurements of the Shielding Effectiveness

This passage details the set-up and methodology used to measure the SE in the semi-anechoic chamber. Afterwards, an analysis of the best configuration is conducted to determine the optimum selection of antennas and antenna/wall distances. It concludes presenting the dynamic range achieved with this method, the maximum SE measurable.

4.1 Assembly Of The Equipment

The process required to prepare the set-up takes around 45 minutes and is summarized down below:

I. Replace manually the original panel by another one with a 315x315mm square aperture and open the inside trapdoor (Figure 23). This is the most time-consuming process.

Figure 23 Aperture of the chamber close/open (up/down) from the outside/inside (left/right)

II. Place the antennas correctly: height, distance to the wall and orientation.

III. Connect the electronic devices; signal generator and network analyzer. The connection and configuration of this equipment will be explained extensively in the next subsection.

The previous steps configure the scenario for the reference measurement. Afterwards, the different plates must be screwed to the frame using a cordless drill/driver and measured one by one without modifying any other parameter of the scenario. In particular, touching the antennas should be avoided to not introduce extra losses due to misalignment.

4.2 Measurement Methodology

Once the setup is ready to initiate the measurements for one plate the evaluation is fully controlled from the computer placed inside the adjoining room (Figure 24).

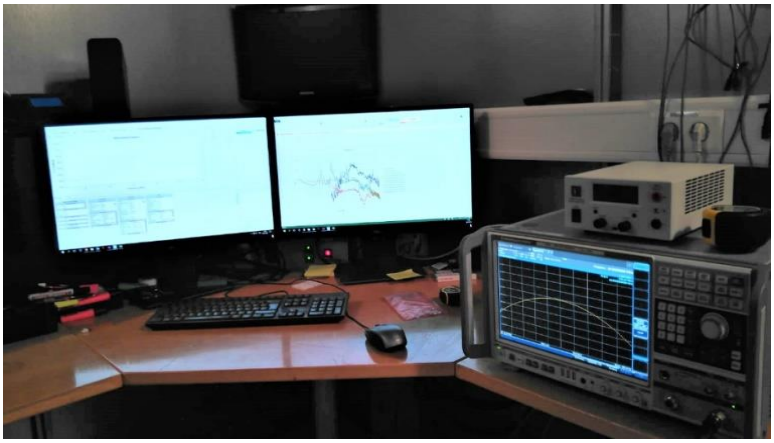

Figure 24 Inside view of the control room

The software installed allows the configuration of parameters like: bandwidth analysed, measure bandwidth, frequency step and output power among others. As well as the visualization of the results referenced to an initial measure (SE), facilitating the detection of incorrect results. A second method to control the data collected is the visual verification using the network analyzer screen:

I. The maximum of the slope must coincide with the middle frequency.

II. The signal received must be at least 6 dB over the noise floor.

The frequential steps over the bandwidth are show in Table 8:

Start Frequency (MHz)	**Stop Frequency (MHz)**	**Frequency Step (MHz)**
1	100	1
100	500	5
500	6000	10

Table 8 Frequency steps of the measurements

Operation of the system (connections shown in Figure 25):

Connection I (Computer/NA): The configuration of the NA is done using a simple application installed in the computer that works as interface between both devices. Once the scan has started the results are sent to the computer and plotted.

Connection II (Network Analyzer/Signal Generator): The signal generator is controlled by the NA to work synchronized during the scan.

Connection III (Signal Generator/Transmitting Antenna): The antenna placed out of the semi-anechoic chamber is directly connected to the signal generator.

Connection IV (Receiving Antenna/NA): The signal received by the antenna placed inside the semi-anechoic chamber is guided to the input of the NA. The discontinuity of the cable is done to evidence that the antenna is connected to a default output of the semi-anechoic chamber designed to avoid leakages.

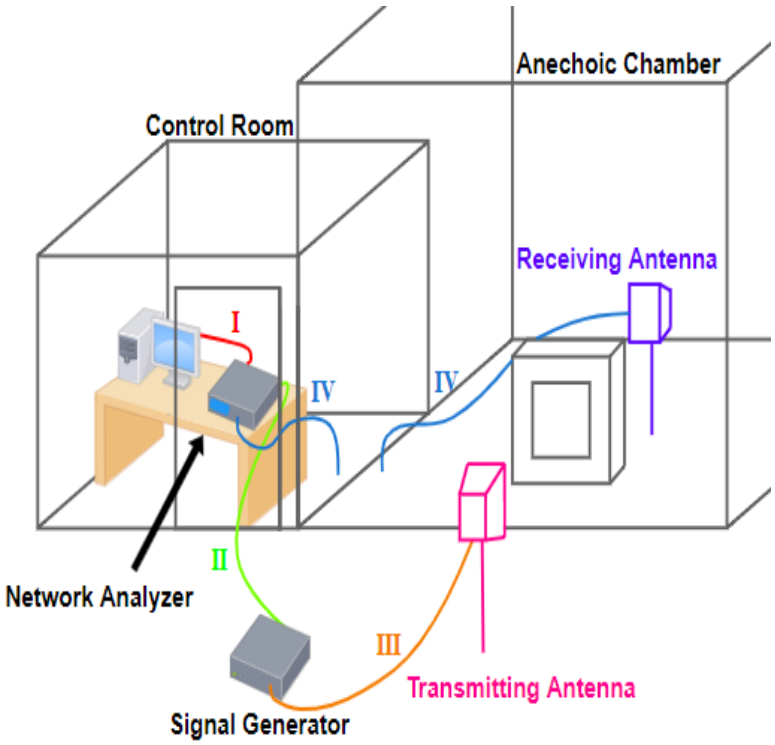

Figure 25 Schematic of the system

This procedure offers a fast scanning of the bandwidth avoiding manual configuration for each frequency. The procedure can be simplified replacing the signal generator by the output of the NA. Nevertheless, this option was discarded because the output power was not high enough.

4.3 Analysis Of The Antenna Distance Effect

This section pretends to stablish experimentally the antenna-wall distance that offers the highest DR. As well as demonstrate the independence between this parameter and the measured SE.

As explained previously, similar measurements had been done before in Seibersdorf Laboratories. In those experiments the distance was set to 50 cm for the Bilog antenna and 55 cm for the Horn antenna, the same configuration will be repeated as a reference.

On the other hand, there is no anterior experience in this type of measurements with the Loop and Biconical antennas. As explained in Chapter 2, there is a standard for the Loop Antenna that suggest using 30 cm. About the Biconical antenna it was decided to set the intermediate value at 150 cm, that is approximately equal to the distance between the wall and the radiant section at low frequencies of the Bilog antenna (Antenna-Wall Distance + Bilog Antenna Length $\simeq$ 50 cm + 100 cm approx. = 150 cm).

Once the intermediate values were chosen, two distances below/under it were decided in the laboratory according to the physical limitations of the semi-anechoic chamber and the surrounding area.

Antenna Type	**Bandwidth Analysed**	**Antenna – Wall Distances**
Loop	1 MHz – 30 MHz	20, 30 & 60 cm
Biconical	20 MHz – 300 MHz	100, 150 & 225 cm
Bilog	30 MHz – 3 GHz	25, 50 & 100 cm
Horn	1 GHz – 6 GHz	22.5, 55 & 110 cm

Table 9 Configuration parameters of the analysis

LPDA is not included in this analysis, the reason is that it has similar characteristics to the Bilog antenna: bandwidth, shape and radiation pattern. Therefore, the effect of the distance in the DR can be assumed to be equal for both. It is a way of making a more efficient use of the time in the semi-anechoic chamber.

Plate Nº9, with a 3mm width aperture and no clamp in the middle of the slot, has been chosen for this analysis (evaluate all the plates with all the antennas would be a waste of time) due to two main reasons:

I. It has a vertical slot, orthogonal to the incident electric field, of approximately 30cm. Consequently, the first resonant frequency appears

at $f = \frac{c}{\lambda} = \frac{c}{2 \cdot L} = \frac{c}{2 \cdot 0.30} \simeq 500\ MHz$. Right in the middle of the range covered by the Bilog antenna.

II. The dimensions of the aperture are large enough to offer a poor SE performance in comparison to other plates. It reduces the chances of working out of the SE dynamic range.

4.3.1 Loop Antenna

The results obtained for the Loop Antenna can be seen in Figure 26:

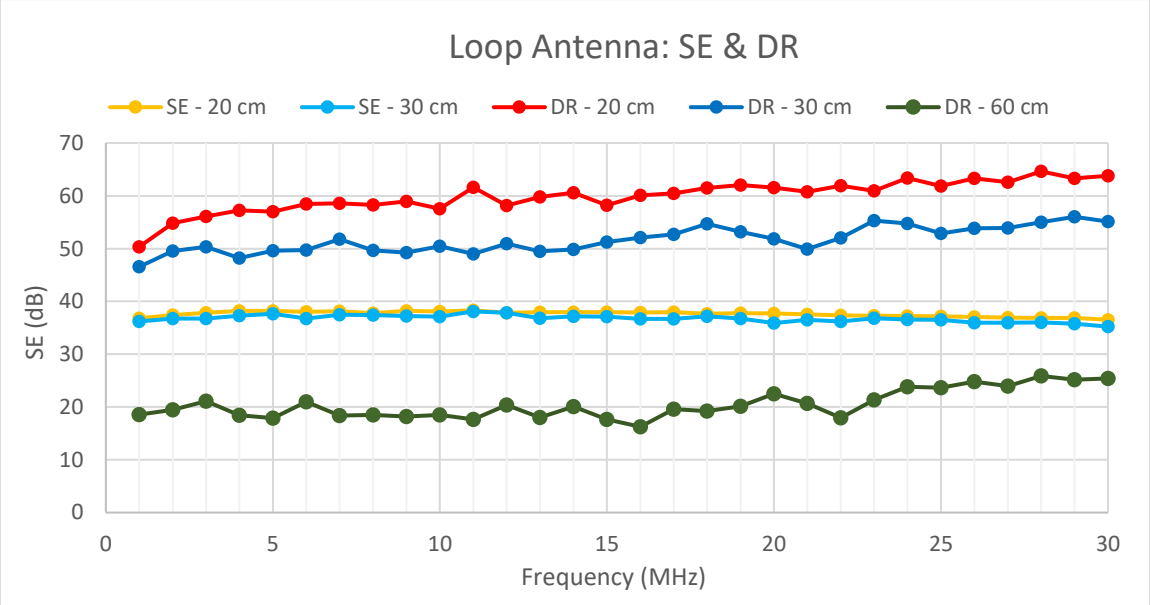

Figure 26 Loop Antenna (Plate Nº9/3mm/No clamp): Effect of the Antenna-Wall distance

Conclusions arising from Figure 26 and the experience in the laboratory:

I. Decreasing the distance increases the DR.

II. Setting the distance to 60 cm produces an extremely low DR that is not enough to measure the SE of the selected plate. This issue was detected during the work in the laboratory (this distance was the last one analysed) and this measurement was skipped.

III. The distance does not affect the SE value.

IV. Working with a very low distance is quite uncomfortable in the laboratory. Although it increases the DR, it also severely complicates changing between plates without moving the transmitting Loop antenna.

According to these results, the most appropriate distance is 30cm. It is the best one in the trade-off: DR/manoeuvrability.

4.3.2 Biconical Antenna

The values measured for the Biconical antenna are presented in Figure 27:

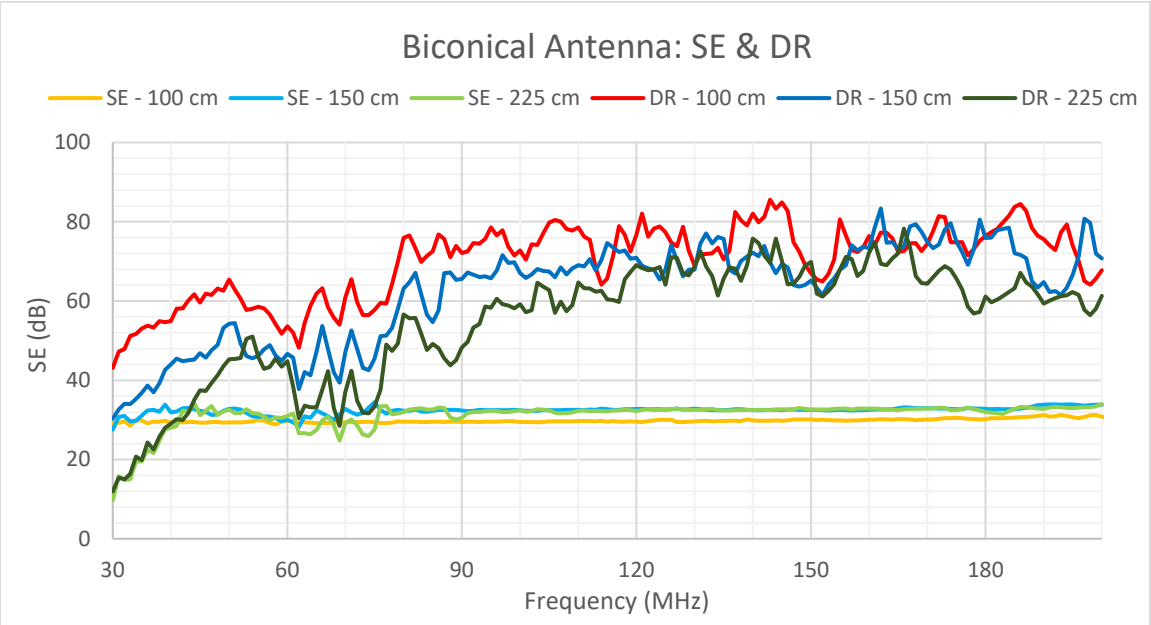

Figure 27 Biconical Antenna (Plate Nº9/3mm/No clamp): Effect of the Antenna-Wall distance

Analysis of the results and the experience in during the tests:

I. The SE is independent of the distance selected, assuming that the value is under the limit stablished by the DR.

II. The DR increases as the distance decreases, being more significant this dependence for the lower frequencies.

III. During the experiments an unsuccessful attempt to decreases the distance was made, but due to the large size of this antenna it was impossible. The antenna was touching the pyramidal RAM that covers the interior surfaces of the semi-anechoic chamber.

The distance finally selected for this antenna is 100 cm.

4.3.3 Bilog Antenna

Figure 28 shows the results corresponding to the Bilog antenna for the distances 25, 50 and 100 cm:

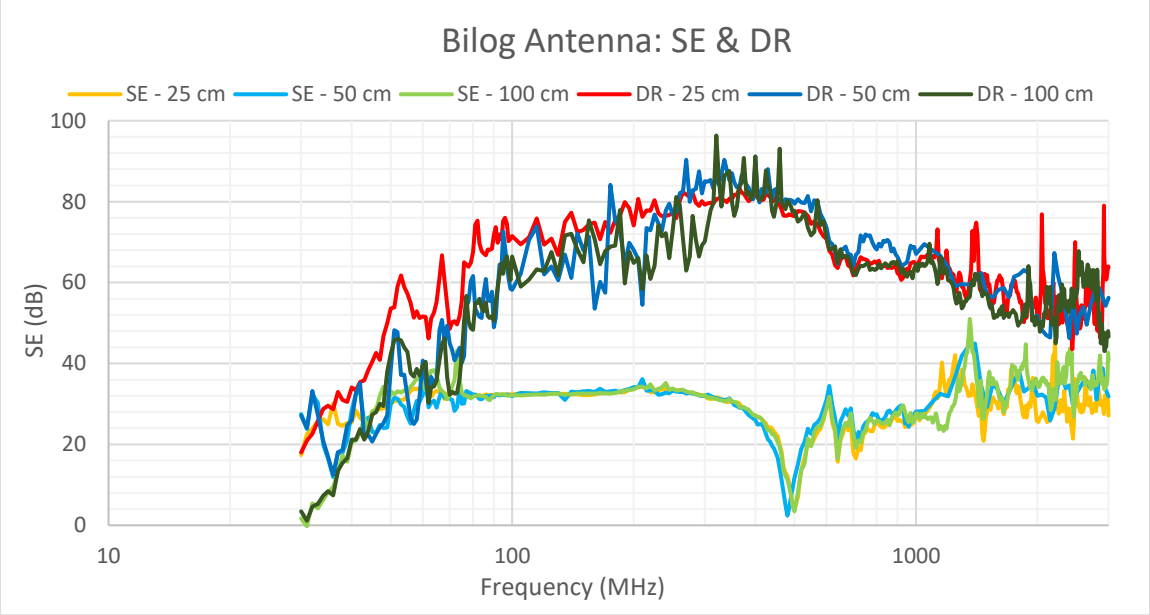

Figure 28 Bilog Antenna (Plate Nº9/3mm/No clamp): Effect of the Antenna-Wall distance

Analysis of the measurements presented in Figure 28:

I. The DR is slightly affected by the distance for frequencies under 200 MHz, over this value the difference among the results is negligible.

II. The measured SE is practically the same in the range analysed. Although the results diverge a bit more for frequencies over 1GHz, this deviation is not large enough to be problematic and does not show a dependence with the distance. The origin of this variations are the resonances produced over 1 GHz, at these frequencies the wavelength is comparable to the set-up dimmensions.

The distance selected is 50 cm. Although for the lower frequencies 25 cm is a better option, its performance is still not good enough and will require the use of another antenna. On the other hand, previous measurements have been done for the distance of 50 cm and the comparison is interesting for the company.

4.3.4 Horn Antenna

The horn antenna results for the distance 22.5, 55 and 110 cm are shown in Figure 29:

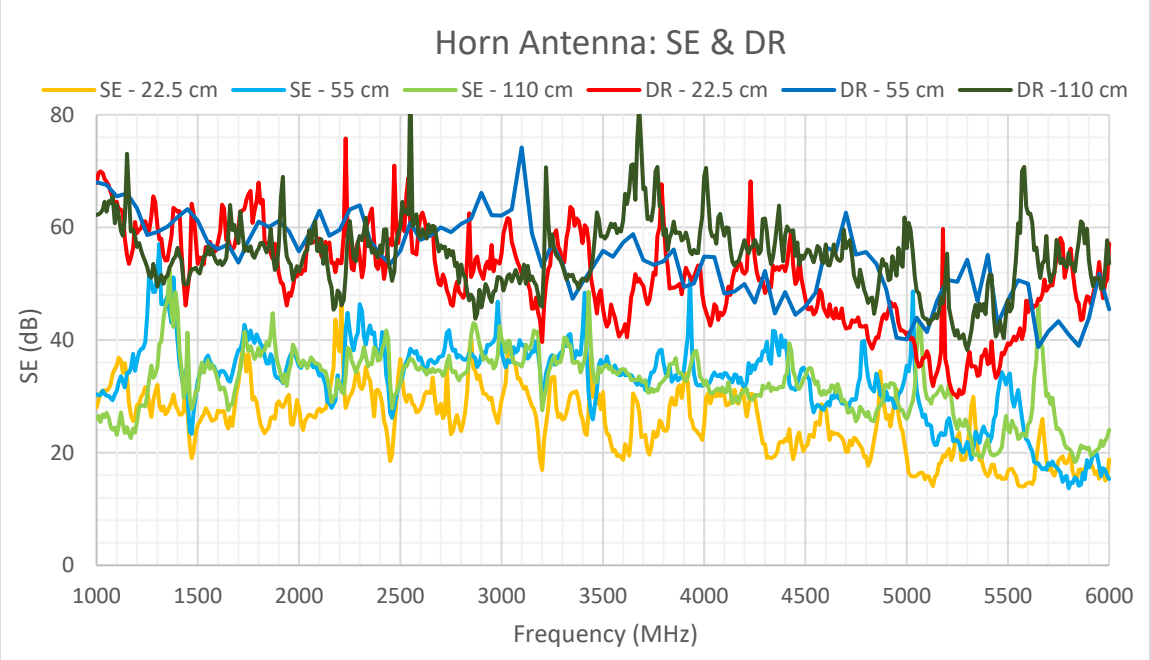

Figure 29 Horn Antenna (Plate Nº9/3mm/No clamp): Effect of the Antenna-Wall Distance

Analysis of Figure 29:

I. DR: the results are very unstable, fast variations with an average of approximately 53 dB that appear to be independent from the distance. Same behaviour we have seen in the results of the Bilog antenna over 1 GHz.

II. SE: these values also present fast variations up to 15 dB. In contrast to the previous point, the distance is affecting one of the measurements. Meanwhile if the distance is set to 55 or 110 cm the results obtained are pretty similar, 22.5 cm offers a 10 dB lower value. The justification of this divergence is the excessive proximity of the antenna in relation to the aperture size. The incident EM wave is not striking the whole opening, the borders are not illuminated due to the high directivity of the antenna. Consequently, the SE measured decreases, it corresponds to a theoretically infinite 3mm width aperture and not to a rectangular opening (30cm x 3mm).

Considering the previous analysis, the distance selected for the following measurements is 55 cm.

4.4 SELECTION OF THE ANTENNAS (30 MHZ – 3 GHZ)

According to the antennas introduced in subsection 3.4, to work in the range 1 MHz – 30 MHz the loop antenna is the only option, as well as the horn antenna is the only one that can cover the bandwidth 3 GHz – 6 GHz. However, from 30 MHz to 3 GHz different antennas can be used. This section pretends to determine the combination that offers the best performance, the maximum DR.

Furthermore, it must be also proved that the measured SE is independent of the antenna chosen. The plate Nº9 with a 1mm width opening and a clamp (1.2 cm length) in the middle of the slot is the one selected for the following reasons:

I. It has two vertical slots, orthogonal to the incident electric field, of approximately 14cm, which implies that the first resonant frequency is located at $f = \frac{c}{\lambda} = \frac{c}{2 \cdot L} = \frac{c}{2 \cdot 0.14} \simeq 1GHz$. At this frequency the resonance can be detected with three antennas: Bilog, LPDA and Horn.

II. As well as in the previous sections, the dimensions of the aperture are large enough to offer a poor SE and work within the dynamic range.

Measurement settings:

Antenna Type	**Bandwidth Analysed**	**Distance Antenna – Wall**
Biconical	20 MHz – 300 MHz	100 cm
Bilog	30 MHz – 3 GHz	50 cm
LPDA	200 MHz – 3 GHz	50 cm
Horn	1 GHz – 6 GHz	55 cm

Table 10 Configuration parameters of the analysis

Due to the large number of traces to plot, the results have been divided in two figures. The first one, Figure 30, shows the results related to the biconical, bilog and LPDA antennas.

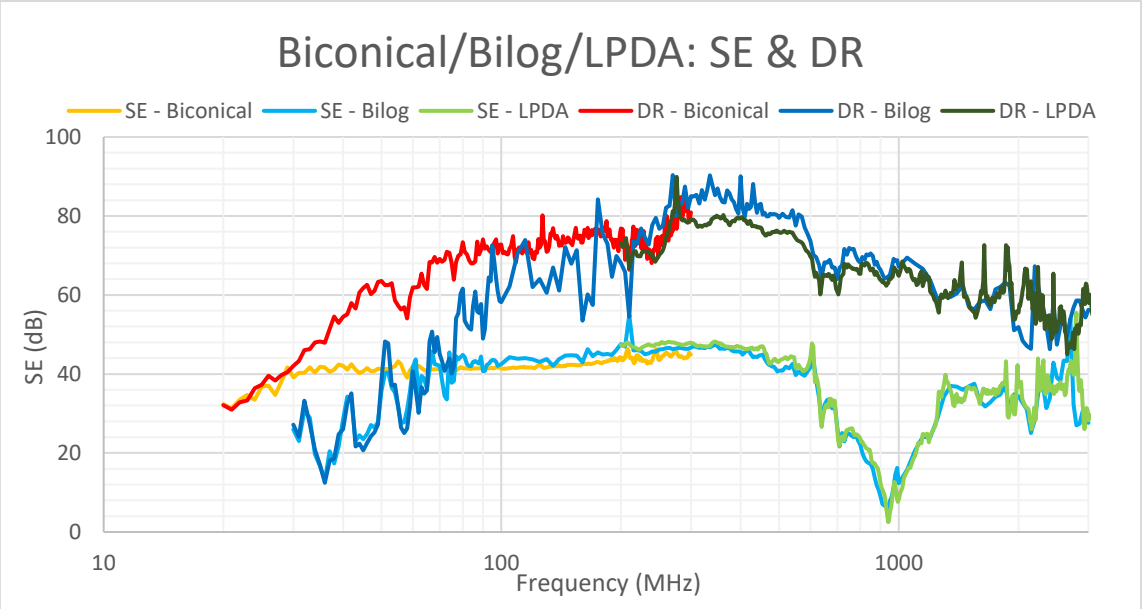

Figure 30 Comparison of Biconical, Bilog and LPDA performance (Plate Nº9/1mm/1.2 cm clamp)

Analysis of Figure 30:

I. DR - Biconical vs. Bilog: In the frequency range [20 - 100] MHz the biconical antenna offers a considerable improvement compared to the bilog antenna, the dynamic range increases around 30 dB. Between 100 MHz and 300 MHz the performance is approximately the same.

II. DR - LPDA vs. Bilog: The DR is almost the same for these antennas between 200 MHz and 600 MHz the Bilog antenna is sligthly better (4 dB approximately).

III. SE: The results do not diverge among antennas, differences of less than 3 dB. It obviously excludes the section in which the SE of the plate is higher than the DR offered by the Bilog antenna.

Conclusions arised:

I. The Biconical antenna has to be used, the DR of the Bilog antenna is too low (below 50 dB) in the range [30 - 100] MHz.

II. LPDA and Bilog antenna can be used indefferently. From now on, only the Bilog Antenna will be used. The reason is that it was already used in previous experiments and the results could be compared, if neccesary.

The second figure of this section, Figure 31, presents the results realted to the Bilog and Horn Antennas.

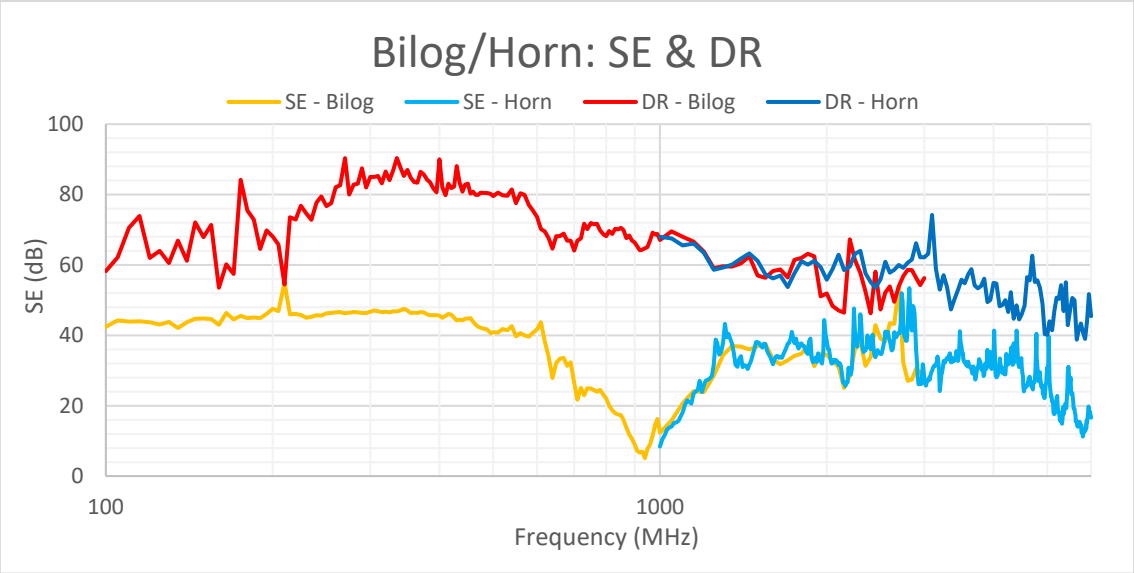

Figure 31 Comparison of Bilog and Horn performance (Plate Nº9/1mm/1.2 cm clamp)

Analysis of Figure 31:

I. DR is practically the same for both antennas in the overlapped range.

II. The SE measured is indeppendent of the antenna used.

4.5 SE Dynamic Range

Figure 32 shows the DR obtained with the configuration selected for the measurements of the plates:

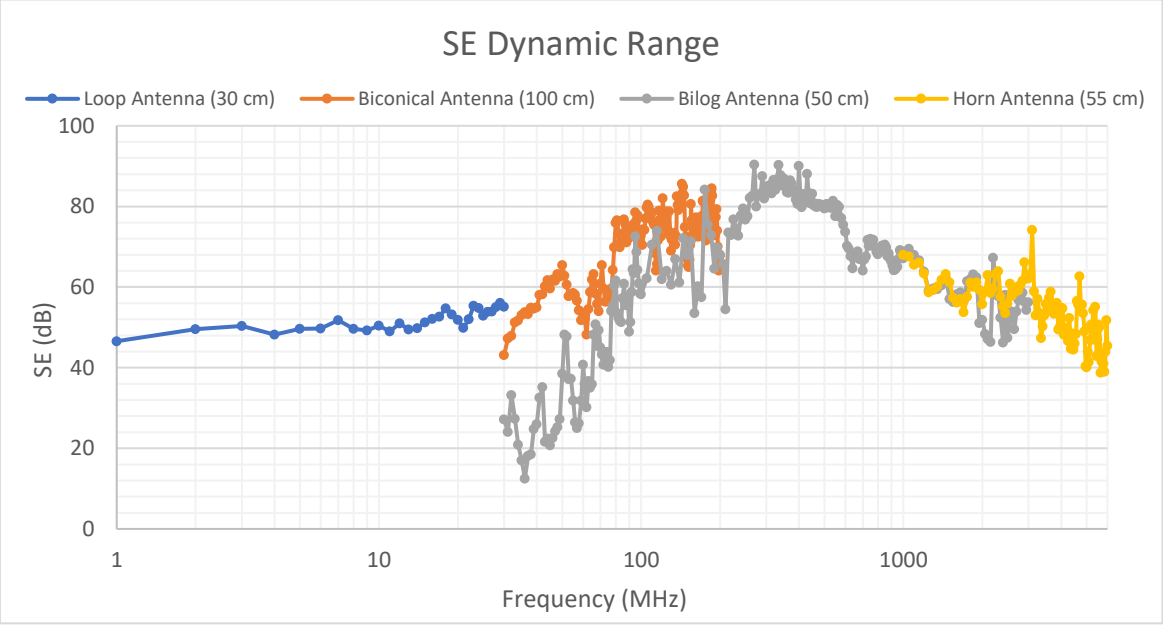

Figure 32 DR of the measuring method (Plate Nº9/1mm/1.2 cm clamp)

The maximum DR obtained for all the frequency range is over 40 dB. Following sections will not contain, to facilitate the visualization of the results,

the measurements corresponding to the Bilog antenna in the overlapped ranges [30-200] MHz and [1-3] GHz. However, these results have been measured in the laboratory. Once the setup is ready, increasing the bandwidth under analysis barely takes a few seconds more, irrelevant compared to the previous preparation of the plate and antennas.

Chapter 5

Numerical Simulation – SEMCAD X

This chapter introduces the simulation software SEMCAD X and its theoretical background. Afterwards, all the information required to develop the simulations is explained: boundaries, materials, models, frequential configuration and EM solver selection.

5.1 SEMCAD X

The software used for this study, SEMCAD X, is a 3D electromagnetic simulation environment based on the Finite-Difference Time-Domain (FDTD) method. This tool offers solutions for the different Technology Computer-Aided Design (TCAD) needs of the wireless and medical sectors: safety assessment, EMI/EMC, antenna design and optimization, 5G, wireless power transfer, dosimetry… [19]

SEMCAD X provides different solvers adapted to specific setups: RF, Low Frequency, EM-thermal simulations…

The last relevant characteristic offered by SEMCAD X is the hardware acceleration. This type of simulations, in function of the model and accuracy, require long runtime periods and memory space. It means that running these calculations in personal computers is not advisable, sometimes even impossible. Special hardware is required as a consequence, since 2009 it is available the use of optimized NVIDIA GPU cards with high bandwidth accelerator memory; it reduces the simulation duration around 35 times. [20]. Figure 33 and Figure 34 show the simulation room in Seibersdorf Laboratories.

Figure 33 Interface with the simulation hardware

Figure 34 Simulation hardware

5.2 FINITE-DIFFERENCE TIME-DOMAIN THEORY

FDTD is one of the most popular and efficient method for the solution of electromagnetic problems nowadays due to three main reasons:

I. It can be applied in a wide variety of situations: scattering, radiation of antennas, optical applications and guided wave propagation among others.

II. It is a time-domain method, which implies that a broad frequency bandwidth can be analysed with just one simulation.

III. It only requires simple mathematical operations: addition, subtraction, multiplication and division.

K. Yee proposed this numerical technique in 1966 and is based on the direct solution of the Maxwell´s curl Equation 5 in the time domain. The original formulas are converted to its finite-difference form and updated following a leap-frog scheme: Electric and magnetic fields components must be alternately calculated in an interlaced spatial grid (Figure 35).

Maxwell´s curl equations
$\nabla x H = \frac{\partial}{\partial t}\epsilon E + \sigma_E E$
$\nabla x E = -\frac{\partial}{\partial t}\mu H - \sigma_H H$

Equation 5

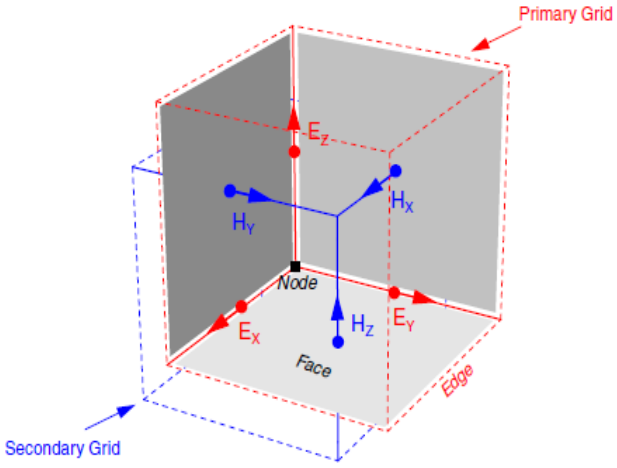

Figure 35 E- and H-field components in the staggered grid [21].

The application of the central differences over the previous equations for the E_x component leads to:

$$\frac{E_x|_{i,j,k}^{n+1} - E_x|_{i,j,k}^{n}}{\Delta t} =$$

$$= \frac{1}{\epsilon_{i,j,k}} \left(\frac{H_z|_{i,j+1/2,k}^{n+1/2} - H_z|_{i,j-1/2,k}^{n+1/2}}{\Delta y} - \frac{H_y|_{i,j,k+1/2}^{n+1/2} - H_y|_{i,j,k-1/2}^{n+1/2}}{\Delta z} - \sigma_{E\,i,j,k} E_x|_{i,j,k}^{n+1/2} \right) \quad \textit{Equation 6}$$

Assuming: $E_x|_{i,j,k}^{n+1/2} = \frac{E_x|_{i,j,k}^{n+1} + E_x|_{i,j,k}^{n}}{2}$. Equation 6 can be reconstructed to obtain$E_x|_{i,j,k}^{n+1}$, the value of the electric field in the next time step:

$$E_x|_{i,j,k}^{n+1} = \left(\frac{1 - \frac{\Delta t \sigma_{E\,i,j,k}}{\epsilon_{i,j,k}}}{1 + \frac{\Delta t \sigma_{E\,i,j,k}}{2\,\epsilon_{i,j,k}}} \right) E_x|_{i,j,k}^{n} +$$

$$+ \left(\frac{\frac{\Delta t}{\epsilon_{i,j,k}}}{1 + \frac{\Delta t \sigma_{E\,i,j,k}}{\epsilon_{i,j,k}}} \right) \left(\frac{H_z|_{i,j+1/2,k}^{n+1/2} - H_z|_{i,j-1/2,k}^{n+1/2}}{\Delta y} - \frac{H_y|_{i,j,k+1/2}^{n+1/2} - H_y|_{i,j,k-1/2}^{n+1/2}}{\Delta z} \right) \quad \textit{Equation 7}$$

The mathematical procedure has been explained for the component E_x, the other five field components can be obtained applying the same concepts to Maxwell´s curl equations [21].

5.2.1 Numerical Stability Conditions

The stability of the algorithm (assuming a rectangular lattice) depends on two factors:

I. Cell size: This limitation is consequence of the numerical dispersion of the algorithm. The speed of a plane wave into the grid is conditioned by the time step, direction and number of cells. The next criterion guarantees a good accuracy [22]:

$$\Delta_{max} \leq \frac{\lambda}{10};\ \Delta_x, \Delta_y, \Delta_z \leq \Delta_{max} \qquad \textit{Equation 8}$$

II. Time Step: If the value is too large, small numerical errors usually grow exponentially. The Courant-Friedrich-Levy (CFL) criterion stablishes the maximum value to avoid this situation [23]:

$$\Delta t \leq \frac{1}{c\sqrt{\frac{1}{(\Delta x)^2} + \frac{1}{(\Delta y)^2} + \frac{1}{(\Delta z)^2}}} \qquad \textit{Equation 9}$$

c: speed of light.

$\Delta x, \Delta y$ and Δz: minimum cell size.

5.3 Boundary Conditions

The computational domain simulated is truncated for simulation to limit its size. SEMCAD X offers four types of boundary conditions that can be applied independently for each side of the mesh [24]:

I. Absorbing Boundary Conditions (ABC): It reduces the reflection of incident fields back into the computational domain by absorbing it (Uniaxial Perfectly Matched Layers (UPML)) or simulating a transparent boundary condition (Analytical). UPML is the one selected among them, the analytical version is based on a high frequency approximation and its use requires that the boundaries are far away from the radiating structures. Meanwhile, UPML is well suited for all simulations and is the one recommended by the software developer. It works adding layers of absorbing material, once the incoming wave reaches the last layer it is reflected highly attenuated. The attenuation depends on its thickness and absorbing profile, it can be configured manually or calculated by SEMCAD X in function of the selected level of strength: low, medium, high or very high.

II. Perfectly Conductive Boundary Conditions: The computational domain is truncated assuming a plane made of perfect electric conductor (PEC). Relevant for this project.

III. Perfectly Magnetic Boundary Conditions: The computational domain is truncated assuming a plane made of perfect magnetic conductor (PMC). Unnecessary for this project.

IV. Periodic Boundary Conditions: It is applied to structures with geometric periodicity. Unnecessary for this project.

5.4 Material Properties

The designed solid regions must have associated material properties, SEM-CAD X provides three different categories: dielectric (including dispersive and non-linear materials), PEC/Metal and PMC. Dispersive/non-linear materials and PMC are not used in this project [25].

Among the numerous options available for the PEC/Metal category, there is one especially relevant: thin resistive sheets (TRS). Meanwhile any other configuration requires 3-dimensional voxels this option accepts 2-dimmensional geometries. It is useful against a common problem of FDTD simulations: small spatial discretization implies small time step (less efficient simulations). TRS ignores the sheet thickness (does not modify the grid) but models its influence. It is of special interest for the modelling of electrically thin structures with significant conductivity [26].

5.5 Models

The models of the semi-anechoic chamber, Bilog antenna and Horn antenna were provided by Seibersdorf Laboratories, all the others were developed by the author of this thesis. Except as otherwise indicated, it must be assumed that the material associated to the model is a PEC.

5.5.1 Semi-Anechoic Chamber

The model is a simplification of the semi-anechoic chamber with the following characteristics:

I. 315 mm x 315 mm square opening modelled without screws and nuts, it reduces the numbers of voxels and can be neglected because its impact in the transmitted power is irrelevant (Figure 36).

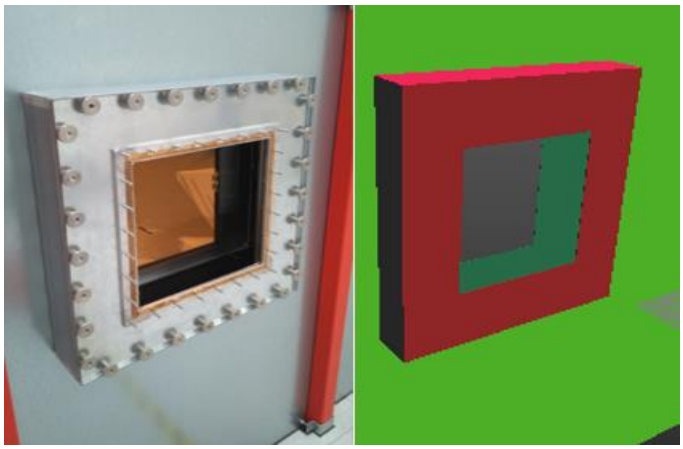

Figure 36 Square Opening: Original vs. Model

II. The boundaries are defined as ABC, except the floor that is a PEC (Figure 37).

III. The limit of the wall matches the boundaries dimensions (Figure 37). It is a simulation trick that makes the wall size equivalent to infinite, no leakage through the borders. The only path between transmitter and receiver is the square opening.

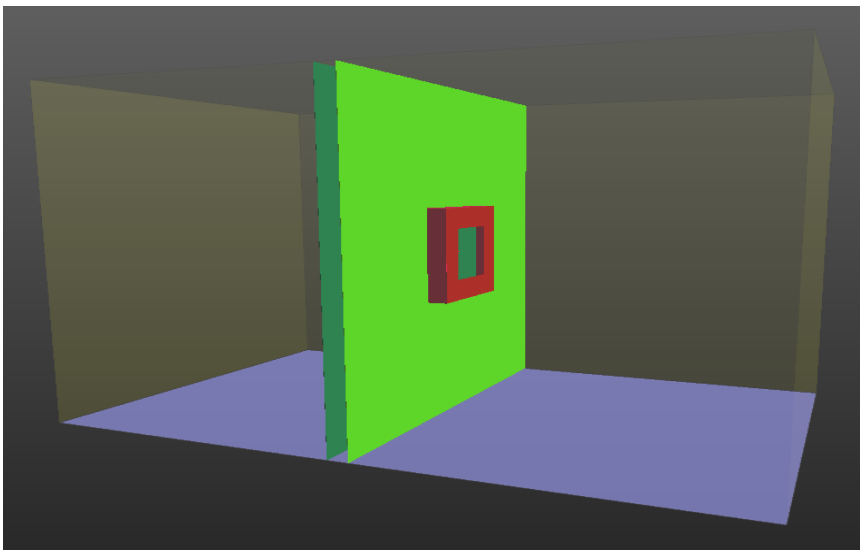

Figure 37 Model of the Semi-Anechoic Chamber

5.5.2 Plates

The comparison between original and model is offered below for all the plates:

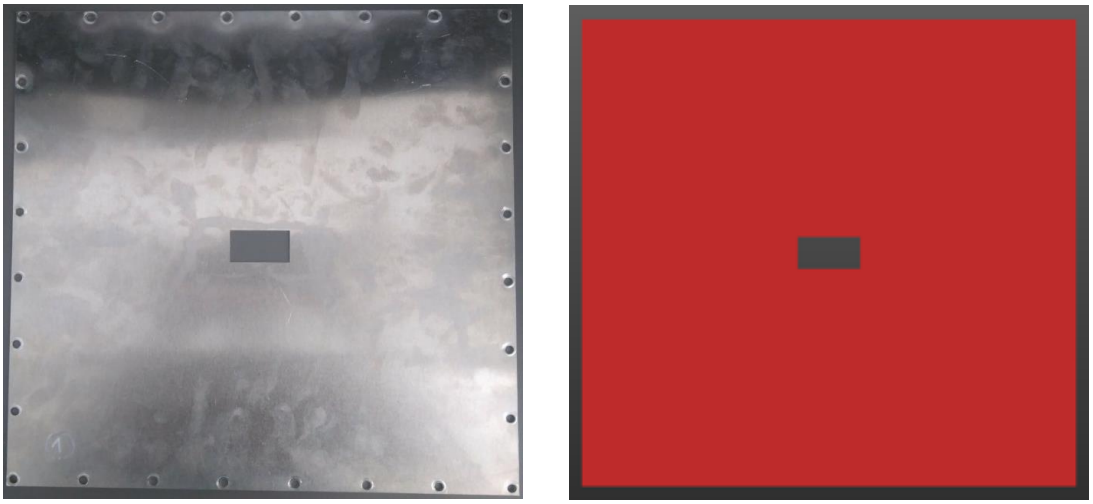

Figure 38 Plate Nº1: Original vs Model

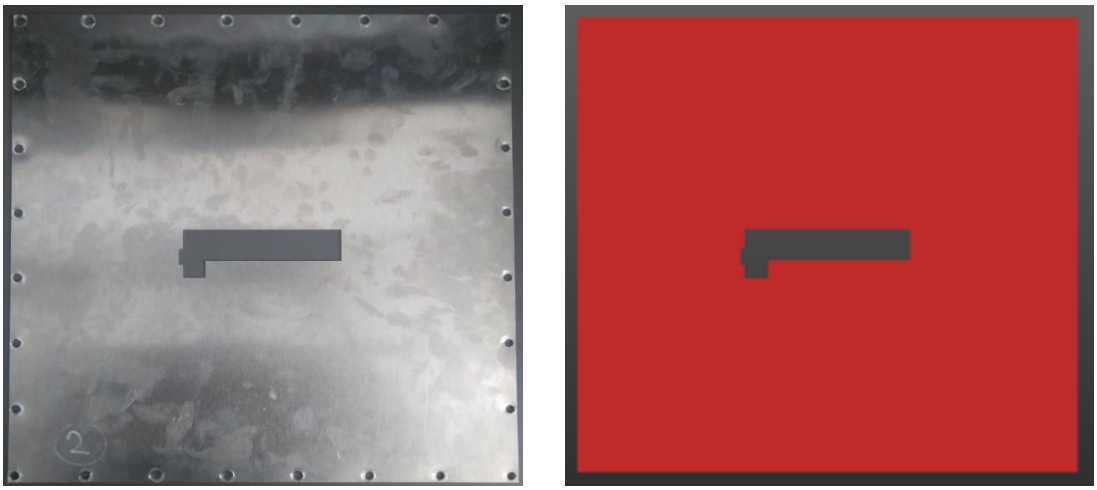

Figure 39 Plate Nº2: Original vs Model

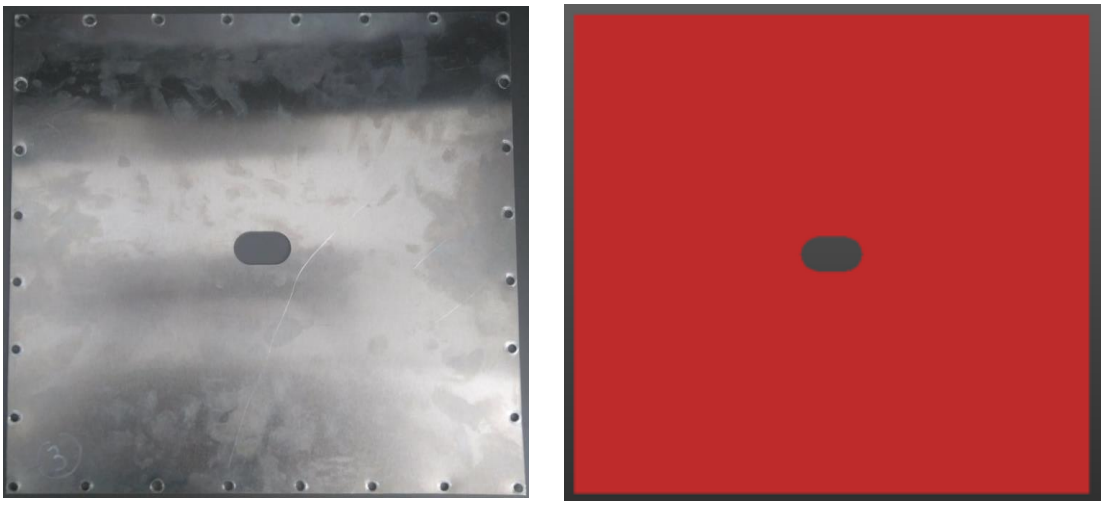

Figure 40 Plate Nº3: Original vs Model

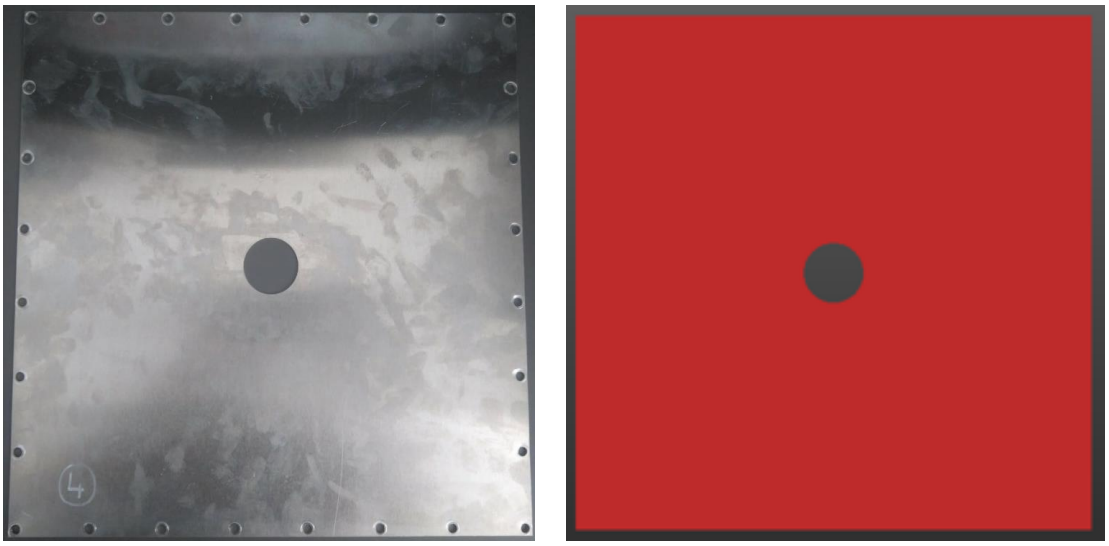

Figure 41 Plate Nº4: Original vs Model

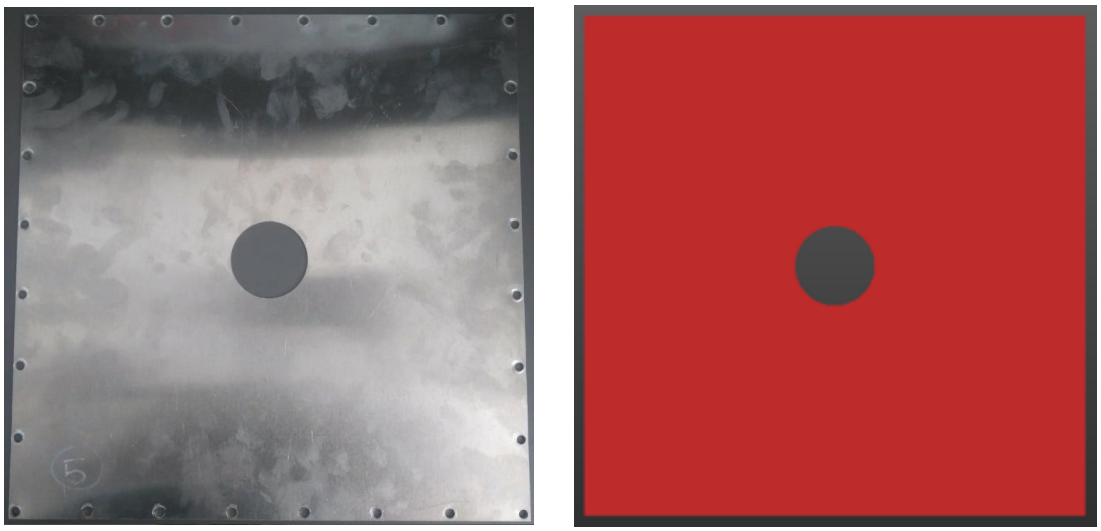

Figure 42 Plate Nº5: Original vs Model

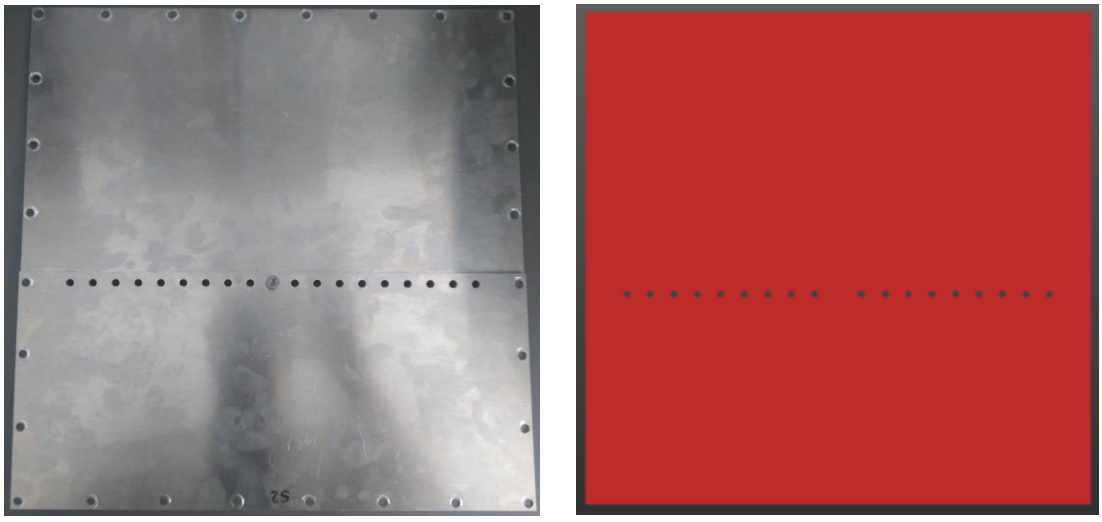

Figure 43 Plate Nº6: Original vs Model

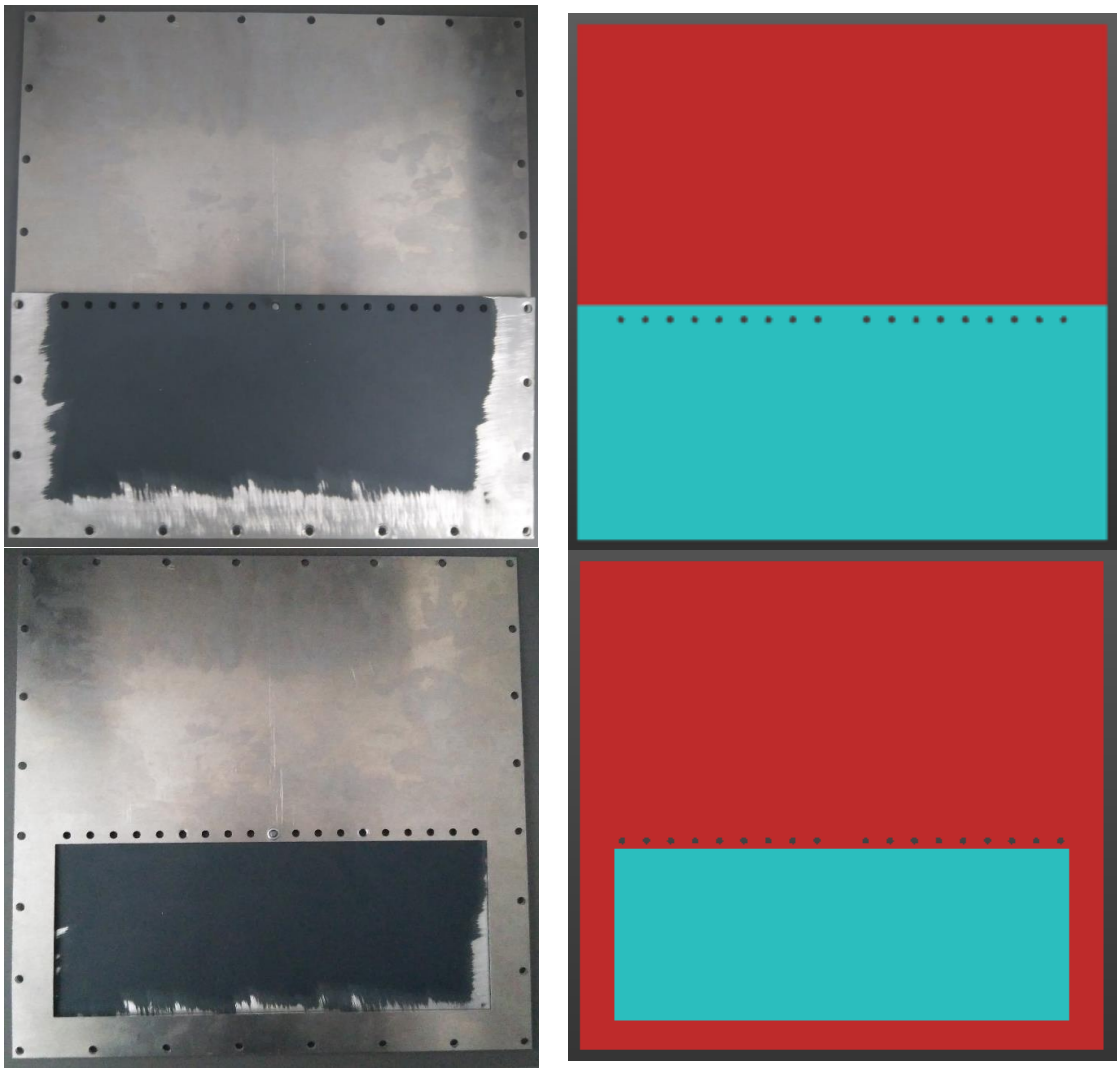

Figure 44 Plate Nº7: Original vs Model

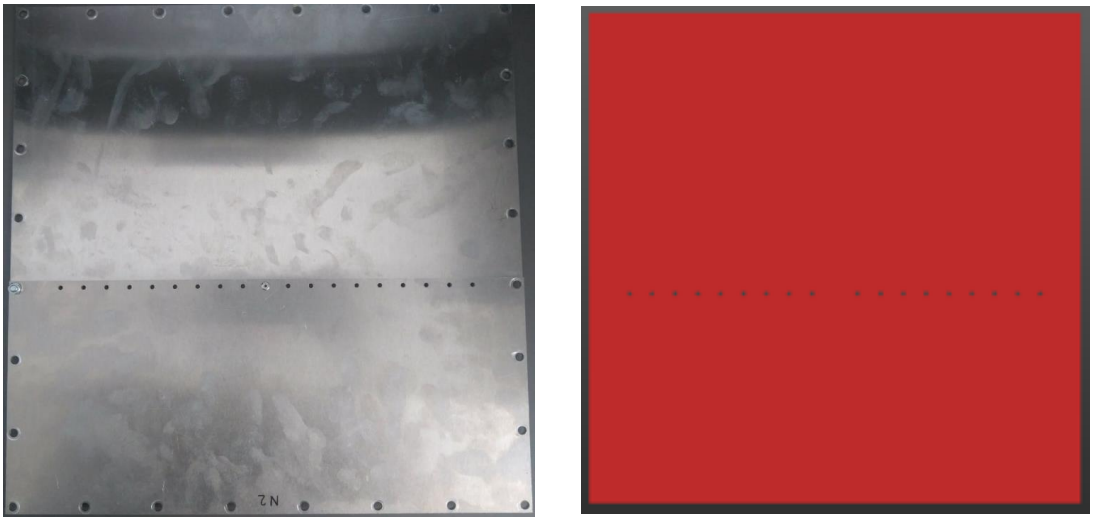

Figure 45 Plate Nº8: Original vs Model

The difference between plate Nº6 (Figure 43) and Nº7 (Figure 44) is the metallic material the smallest rectangular sheet is made of (blue colour in Figure 44): it is a different metallic material covered with a layer of paint (no information about its electromagnetic properties was provided).

The small rectangular sheet in Plates Nº6 and Nº8 (Figure 45) was defined as a PEC, in plate Nº7 as a lossy metal that was simulated for different electrical conductivities. The model assumes a perfect connection between both sheets.

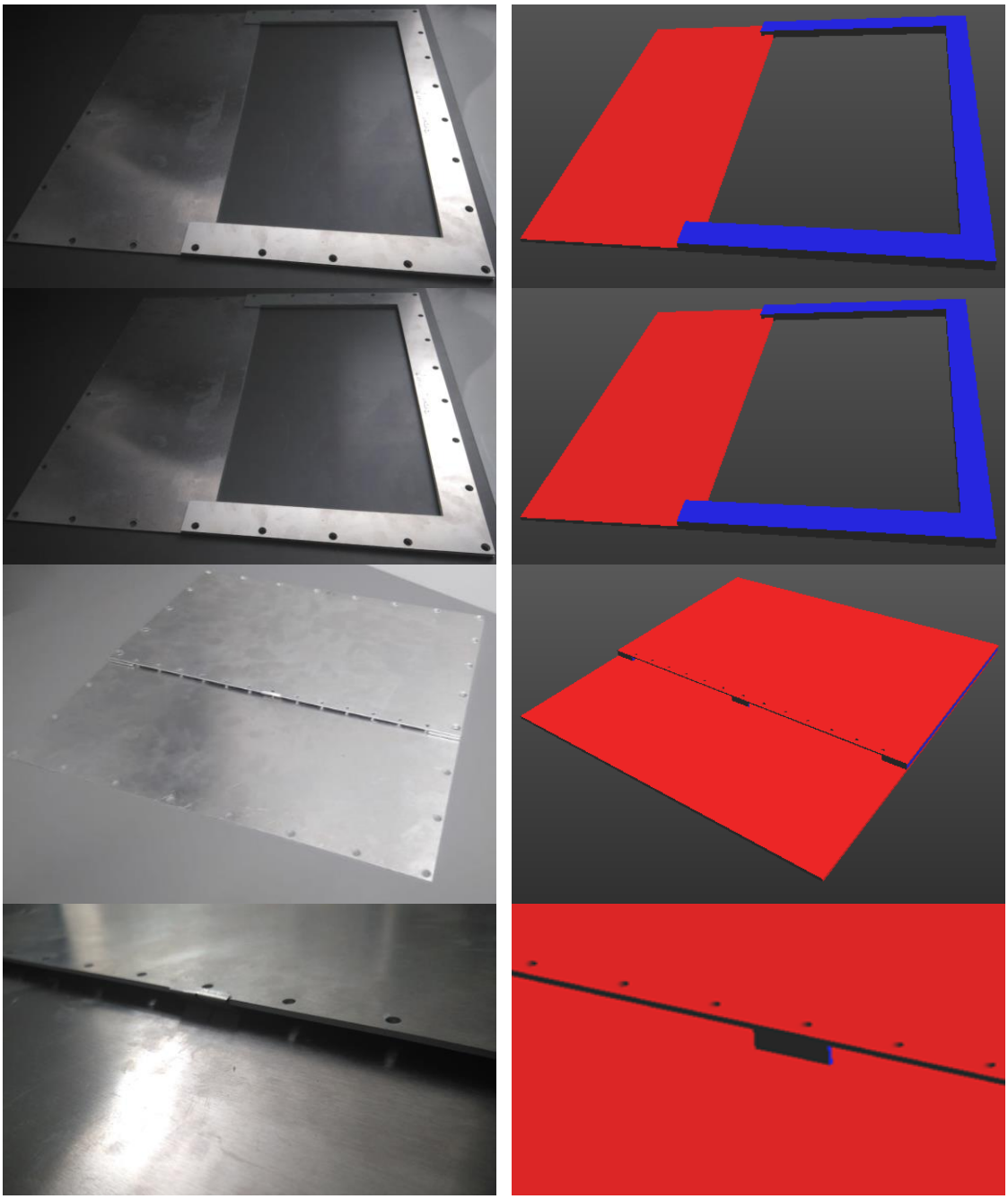

Figure 46 Plate Nº9: Original vs Model

Plate Nº9 (Figure 46) is fully modelled as a PEC and the connections between the different layers is assumed to be perfect. The opening width has been evaluated for 1, 2 and 5 mm. The EMC clamps electromagnetic behaviour is unknown. The model approximates its performance to a PEC rectangular cuboid: 1 mm height, 12/20 mm width and 1/2/5 mm depth. Comparison between results and simulation will show if this simplification is suitable.

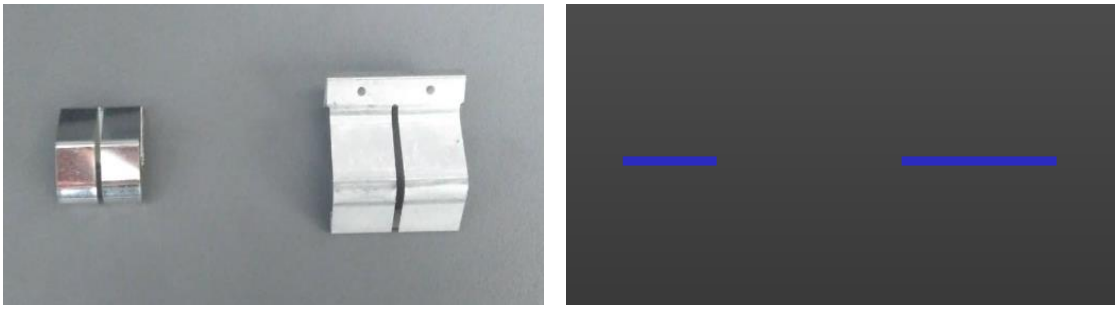

Figure 47 Connectors: Originals vs Models

Plate Nº10 (Figure 48) contains a drilled net of unknown electromagnetic properties. This structure has been modelled initially in two different ways: TRS with a high electrical conductivity (enough to behave as a PEC) and a 1 mm thick PEC.

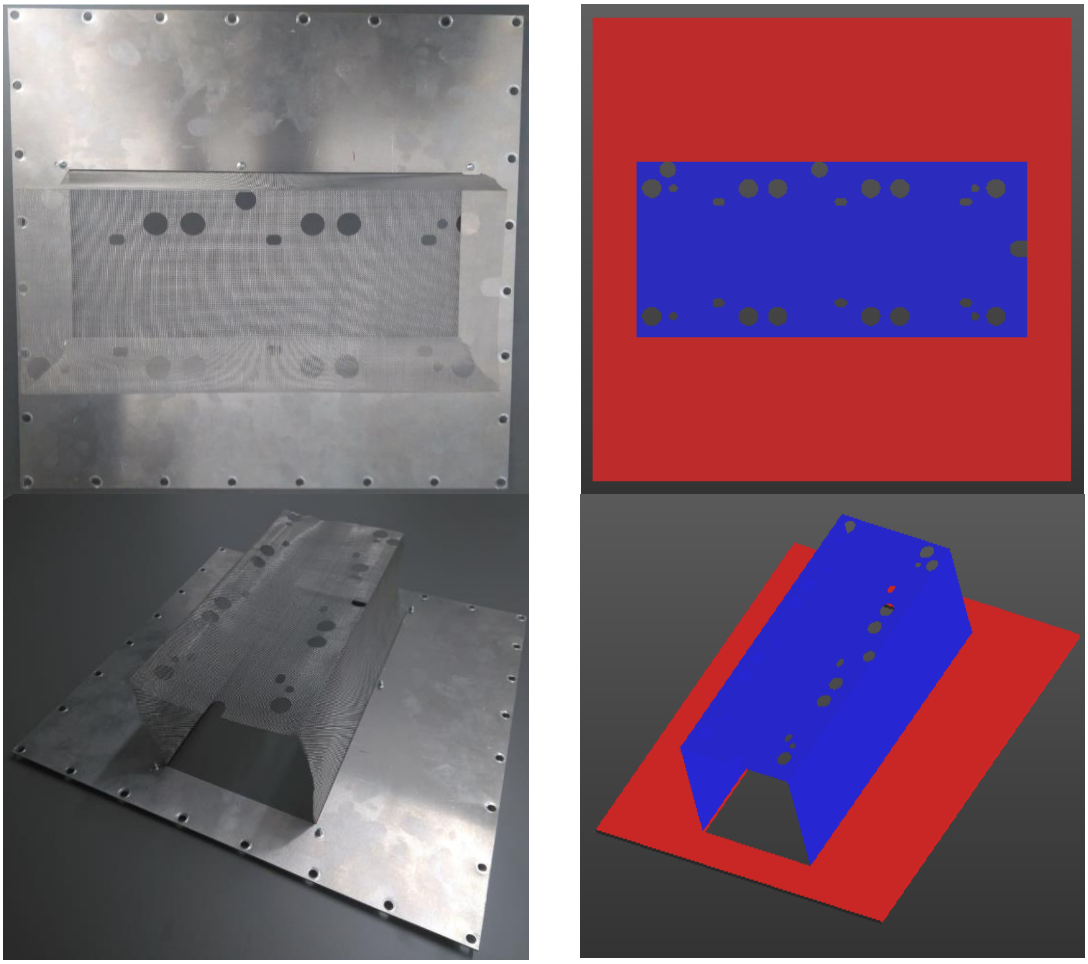

Figure 48 Plate Nº10: Original vs Model

5.5.3 Antennas

Loop, Bilog and Horn antennas have models that assume PEC materials:

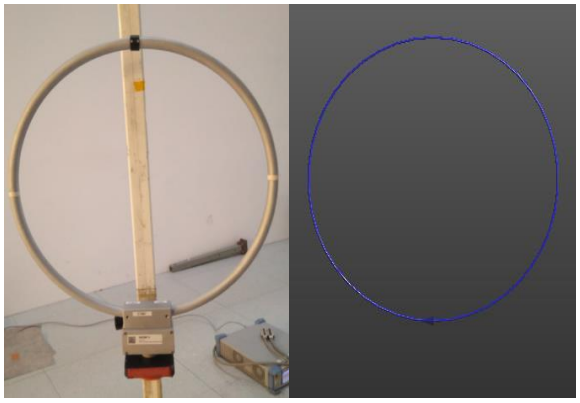

Figure 49 Loop Antenna: Original vs Model

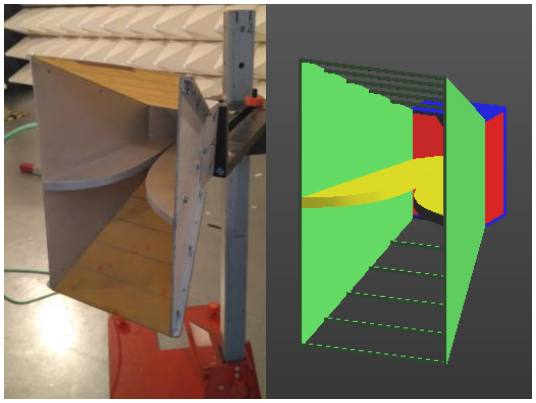

Figure 50 Horn Antenna: Original vs Model

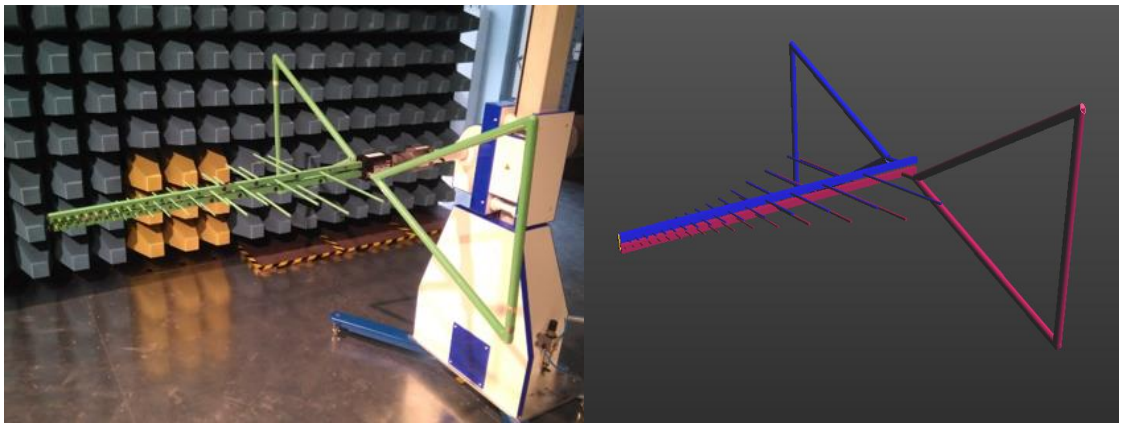

Figure 51 Bilog Antenna: Original vs Model

The Biconical antenna has not been modelled for two main reasons:

I. Simulations started before doing the first measurements, the semi-anechoic chamber was being used for other projects and, therefore, unavailable. At this point the use of the Biconical antenna was not planned because the Bilog antenna was supposed to cover the frequency range [30 MHz – 200 MHz]. As explained in subsection 4.3, Bilog antenna performance at these frequencies was poor during the initial measurements and the Biconical antenna had to be used.

II. Measurements proved the independence between the SE measured and the antenna used (Biconical/Bilog), the same should happen in simulation. Furthermore, in simulation the low performance of the Bilog antenna is irrelevant because there is no background noise or leakage. Hence, there is no need to model the biconical antenna and increase the number of simulations as the ones already executed with the Bilog antenna should offer equivalent results.

5.6 Simulations Configuration And Voxel Verification

Executing the analysis for a frequency range requires selecting the broadband excitation option. In this mode the source generates a gaussian sine pulse which frequential characteristics must be configured. There is just one requirement to accomplish, simulation time must be longer than the duration of the emitted signal oscillations. The specific settings for each simulation are show in Table 11:

	Loop Antenna	**Bilog Antenna**	**Horn Antenna**
Excitation	Broadband	Broadband	Broadband
Frequency Range	1 MHz – 30 MHz	30 MHz – 1 GHz	1 GHz – 6 GHz
Simulation Time	10 Periods	100 Periods	200 Periods

Table 11 Simulations Settings

The number of periods is related to the middle frequency of the bandwidth: 15.5 MHz, 515 MHz and 3.5 GHz.

The next step is to compute the grid and make the voxels for the simulations. An unexpected issue was found during this process, apertures smaller than 5 mm were not properly created. The voxels generated were too big and the original hole (Figure 52) was closed after the discretization (Figure 53). It was fixed by manually reducing the maximum cell size of the problematic solid regions (Figure 54). It was especially detrimental for Plates Nº 6, 7, 8 and 9.

Figure 52 Model with 3mm Ø holes

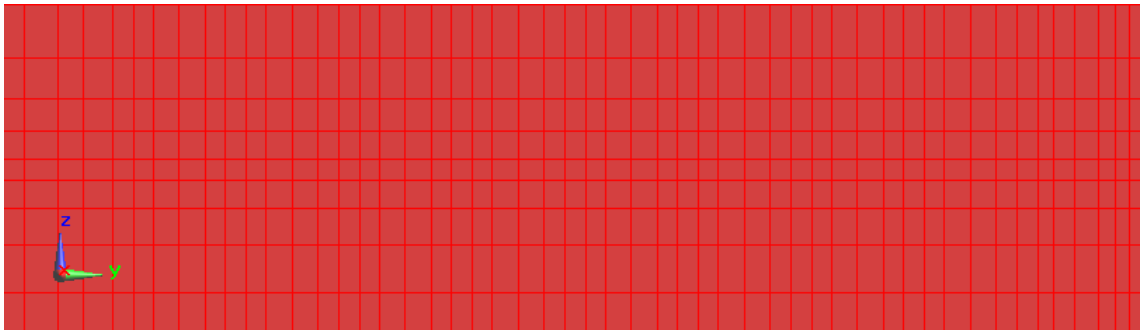

Figure 53 Voxels of Figure 52 without cell size limitation

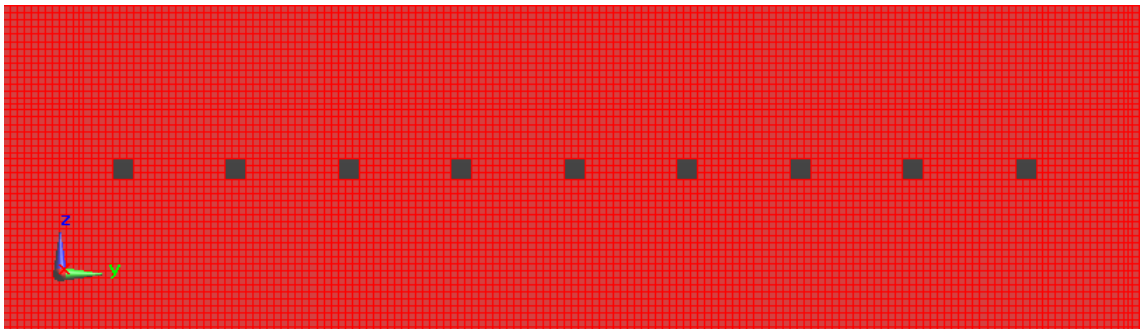

Figure 54 Voxels of Figure 52 with cell size limitation

5.7 EM Solver

SEMCAD X offers three EM solvers:

I. Low frequency.

II. FIT/C-FDTD: Finite Integration Technique (conformal) FDTD.

III. FDTD.

The low frequency solver is not adequate because the analysis pretends to cover a wide frequency range, up to 6 GHz.

On the other hand, FIT/C-FDTD offers more geometrical details than the conventional FDTD. Nevertheless, the TRS algorithm is not compatible with this solver.

Hence, the optimum solver for this project is the standard FDTD. It is a general-purpose solver well suited in the RF frequency range. The disadvantage is that its performance decays for very low frequencies [27].

Chapter 6

Evaluation and Improvement of the Results

This section presents the SE values obtained during the investigation. The analysis of the results is done in two different ways. Firstly, the effect of aperture size/shape, EM clamps and material in the measured SE is studied and justified. Afterwards, the concordance with the simulations is verified. Last subsection offers a solution for one of the issues found during the results analysis: lack of concordance between simulations and measurements in the frequency range [30 MHz – 200 MHz].

6.1 Plates №1 & №3: Aperture Size/Shape Effect

Firstly, the results of each plate will be plotted and analysed separately. Afterwards, due to the aperture shape and size similarity (Figure 55), the measurements will be compared to evaluate the effect of modifying these parameters.

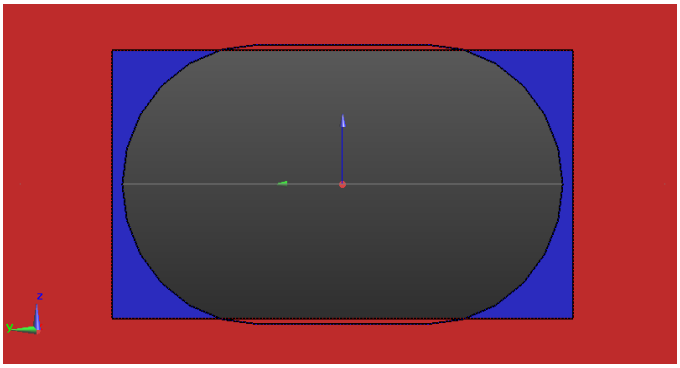

Figure 55 Apertures of Plates №1 (Red) and №2 (Blue)

In both cases, the electric field component is confined in the y-axis (Green vector in Figure 55) (Excluding the Loop Antenna). Hence, the first resonance (according to subsection 2.4) is determined by the aperture size along the z-axis (Blue vector in Figure 55):

$$f = \frac{c}{\lambda} = \frac{c}{2 \cdot L} \simeq \frac{c}{2 \cdot 0.025} \simeq 6\ GHz \qquad \textit{Equation 10}$$

Simulations results are plotted as a single line, without differencing between antennas. The purpose of this is to offer a better visualization of the values. The broadband division for the simulations was defined in subsection 5.6, Table 11.

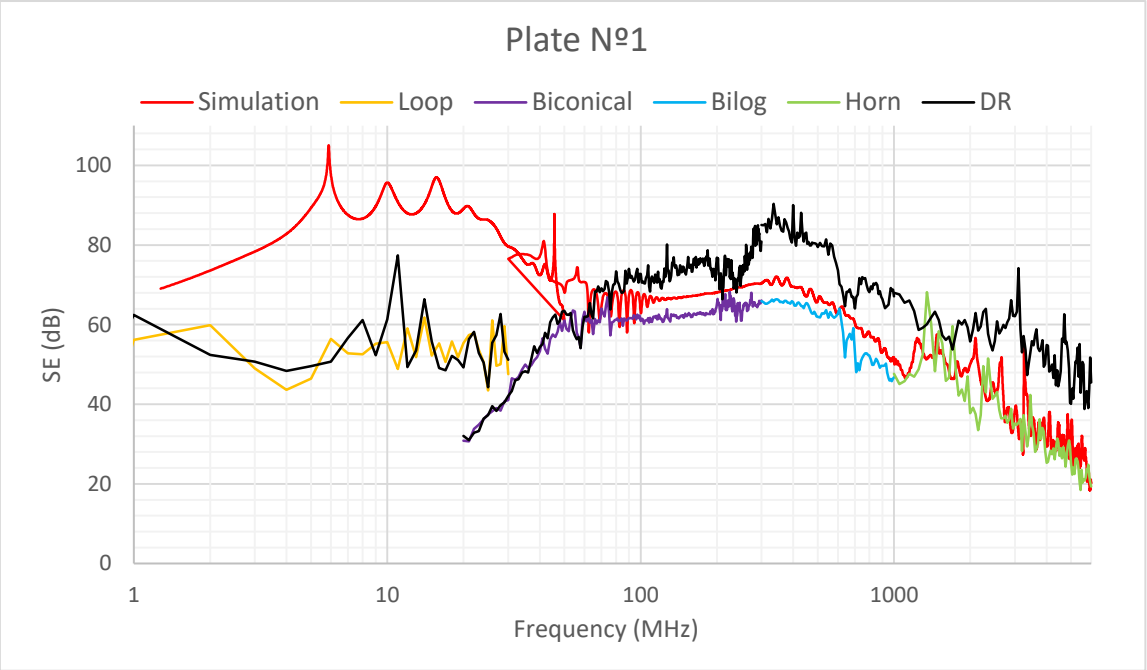

Figure 56 Results of Plate Nº1

Analysis of the measurements:

I. The SE value for frequencies under 100 MHz is equal to the DR. Therefore, the real SE cannot be determined, it is higher than the limits of the system.

II. Over 100 MHz, the SE decreases as the frequency increases. The minimum is located at 6 GHz, as expected.

Analysis of the simulations:

I. 100 MHz – 1 GHz: The simulations results have a constant deviation of 4 dB. This slight divergence is irrelevant when the SE is so high (>60 dB).

II. 1 GHz – 6 GHz: There is no constant deviation, but at certain frequencies there is a deviation higher than before. The reason is that at high frequencies the wavelength is comparable to the scenario dimensions, and unexpected resonances can appear in the measurements. However, in general, the simulation fits better the measures.

Plate Nº3 results:

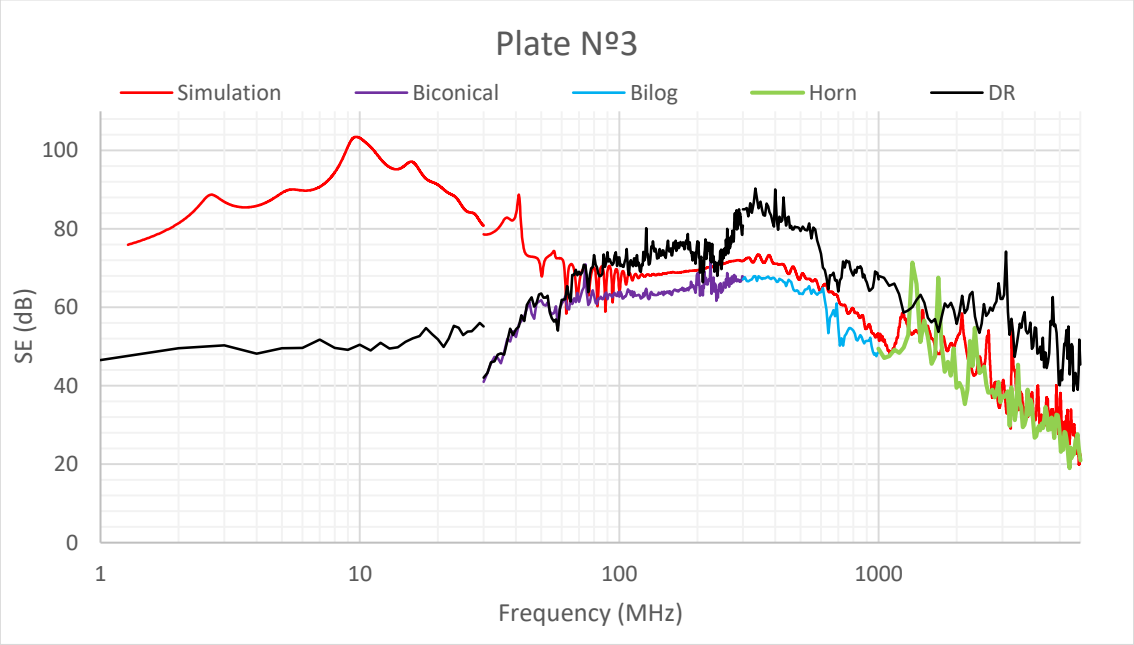

Figure 57 Results of Plate Nº3

The high similarity between both apertures, as mentioned previously, leads to equivalent conclusions. Hence, the analysis elaborated for Plate Nº1 is also suitable for this case.

There is no measure of the Loop antenna because it was considered unnecessary and a waste of time. The DR would be, as happened with Plate Nº1, lower than the real SE.

The graph down below, Figure 58, stablish a comparison of the measures obtained for each plate:

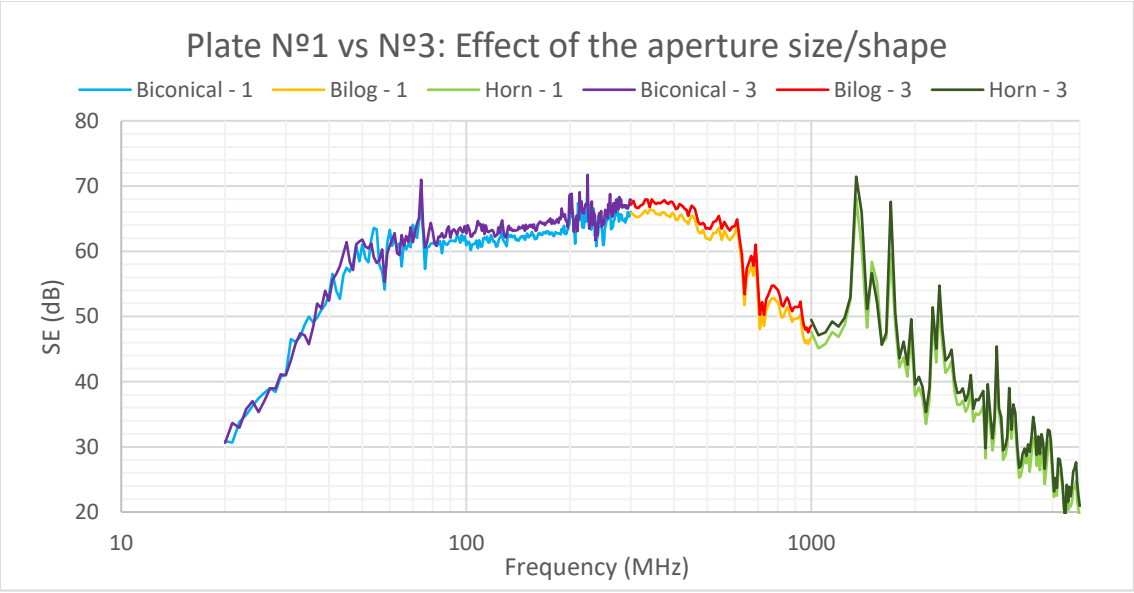

Figure 58 Comparison between the measurements of Plates Nº1 and Nº3

These measurements are practically indistinguishable, just a small offset of approximately 3 dB appears in the frequency range [100 MHz – 1 GHz]. However, this divergence is not high enough to be relevant. In other words, the slight differences between Plates Nº1 and Nº2 have no impact in the SE.

6.2 Plate Nº2: Orientation Effect

According to subsection 2.4, SE depends on the maximum linear dimension of the aperture that is perpendicular to the electric field. Plate Nº2 has been measured in two different orientations (Figure 59) to evaluate this effect.

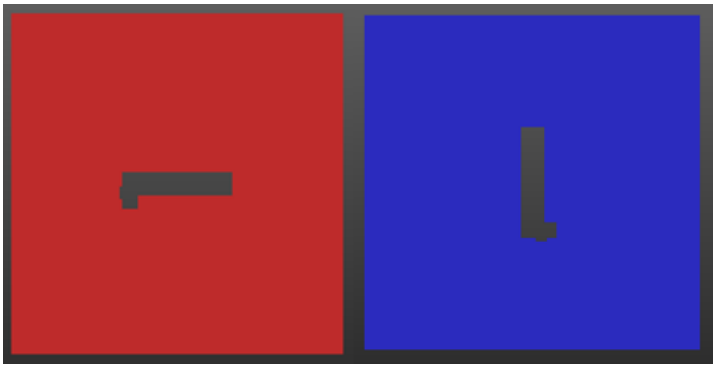

Figure 59 Plate Nº2 Orientation: Horizontal (Red) vs Vertical (Blue)

First harmonic for each orientation according to Figure 59 and assuming horizontal incidence of the electric field:

$$Horizontal:\ f = \frac{c}{\lambda} = \frac{c}{2 \cdot L} \simeq \frac{c}{2 \cdot 0.024} \simeq 6.25\ GHz \qquad \textit{Equation 11}$$

$$Vertical:\ f = \frac{c}{\lambda} = \frac{c}{2 \cdot L} \simeq \frac{c}{2 \cdot 0.117} \simeq 1.28\ GHz \qquad \textit{Equation 12}$$

The results have been plotted in Figure 60. There is no different trace for each antenna, as previously, to simplify the graph. However, the broadband division is equivalent to the one done in the preceding subsection.

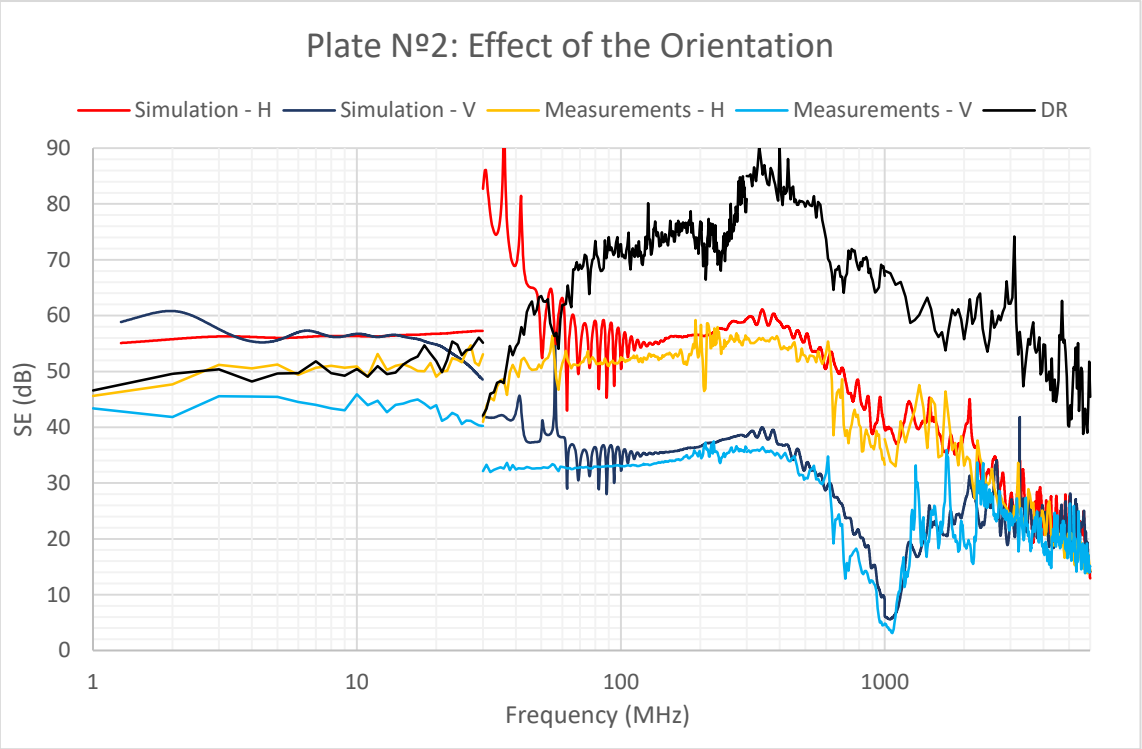

Figure 60 Results of Plate Nº2

Analysis of the measurements:

I. SE measured by the Loop antenna for the horizontal orientation is limited by the DR, those data cannot be taken into consideration. Despite this, it is obvious that the SE for the vertical alignment is lower. This difference is unexpected, theoretically the Loop antenna generates a magnetic field perpendicular to the plate and, therefore, the measure should be independent of the orientation. The divergence could be produced by the miscalibration of the set-up between scans, the floor (the scenario between orientation is not symmetric due to the floor), or another unknown factor. Unfortunately, this measurement could not be repeated after detecting this issue and no justification has been found.

II. The horizontal orientation has its minimum slightly above 1 GHz, close to the predicted 1.28 GHz. On the other side, the vertical orientation has its SE minimum in the highest frequency analysed (6 GHz), this is in line with the harmonic calculated at 6 GHz.

III. Under 1 GHz the orientation introduces an offset between traces close to 20 dB, but it does not modify the shape of the line. Over 1 GHz the offset begins to decrease progressively until it becomes practically null at 3 GHz. These results suggest that the orientation has a big impact when the wavelength is large in relation to the aperture size. If the wavelength is comparable the orientation becomes irrelevant.

Analysis of the simulations:

I. Loop antenna: the obtained values are quite similar for both orientations (as expected), the slight differences can only be attributed to the floor. However, it does not fit the measures in this range. Up to this point, the Loop antenna simulations have not been compared to measurements because the DR has been a limitation, but it has been done for following plates with successful results. It means that the model of the Loop antenna is appropriate, the origin of the mismatch is in the measure.

II. [30 MHz – 100MHz]: The simulation results are higher than the measurements and with important oscillations. It is a recurrent problem for the Bilog antenna simulations in this frequency range. A solution for this mismatch is offered at the end of this chapter.

III. Over 100 MHz the simulation predicts with high accuracy the results obtained in the laboratory, except for certain resonances at high frequencies (>800 MHz).

6.3 PLATES Nº4 & Nº5: DIAMETER SIZE EFFECT

This subsection is going to analyse the influence in the SE of the diameter size using Plates Nº4 and Nº5 (Figure 61). It is of main importance the evolution of this factor with the frequency.

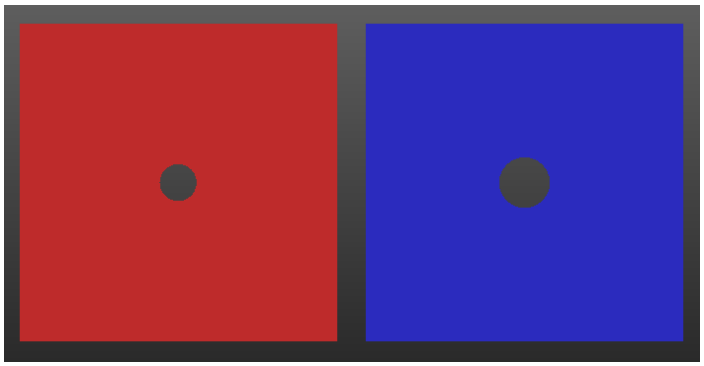

Figure 61 Plates Nº4 (Red) and Nº5 (Blue)

First resonances for each plate assuming a linear polarization of the electric field:

$$Plate\ Nº4\ (40\ Ø\ \text{mm}):\ f = \frac{c}{\lambda} = \frac{c}{2 \cdot L} \simeq \frac{c}{2 \cdot 0.04} \simeq 3.75\ GHz \qquad \text{Equation 13}$$

$$Plate\ Nº5\ (55\ Ø\ \text{mm}):\ f = \frac{c}{\lambda} = \frac{c}{2 \cdot L} \simeq \frac{c}{2 \cdot 0.055} \simeq 2.72\ GHz \qquad \text{Equation 14}$$

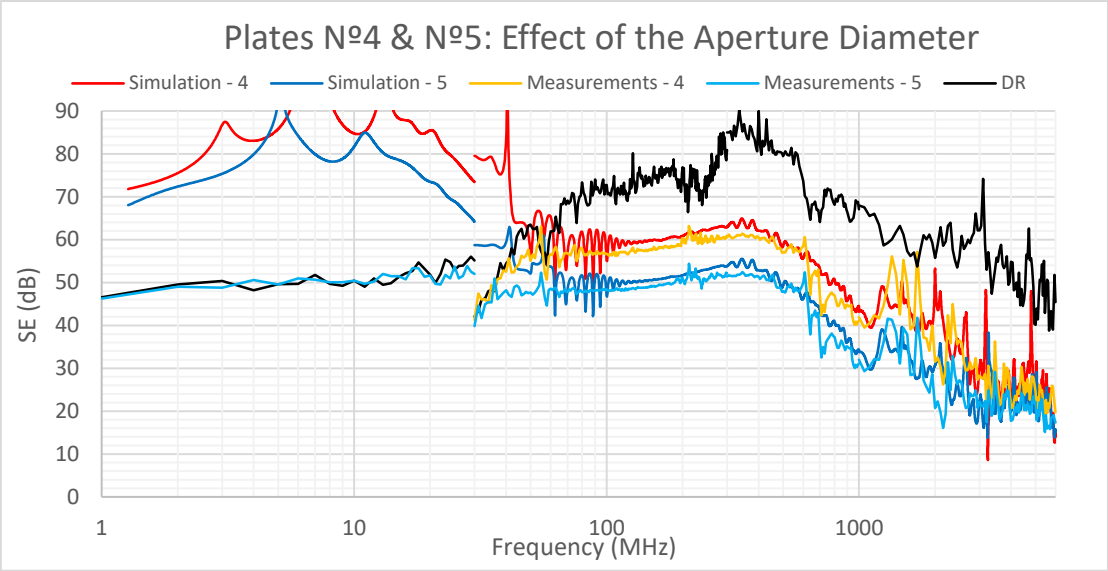

Figure 62 Results of Plates Nº4 and Nº5

Analysis of the measurements:

I. DR for the Loop antenna is too low for this plate. Once it was verified for the plate with lower SE (Nº5) was not necessary to repeat it with the other one.

II. Under 2.7 GHz there is a constant SE offset close to 10 dB. The effect of the diameter size decrease over this frequency, SE is almost the same for both plates. As happened in subsection 6.2, when the wavelength is comparable to the dimensions of the aperture the effect of this parameter tends to disappear.

III. Over 800 MHz certain resonances that does not match the expected ones are visible. These oscillations are equal for both plates, which means that are not consequence of the diameter size. It is probably due to the set-up configuration. On the other hand, the expected resonances at 2.72 GHz and 3.75 GHz do not appear in the graph. The reason is that the equation used assumes that the aperture is perpendicular to the electric field, which is the case of rectangular openings. Circular openings do not have this characteristic and, therefore, the formula is not applicable.

Theoretical justification of the previous statement: The variation in the linearity of the currents induced by the electric field is directly related to the resonance of the slot, higher variations implies higher resonances [2]. Figure 63 shows the effect of the opening shape in the currents. Meanwhile the circular slot modifies the current gradually, the rectangular slot implies a sharper change.

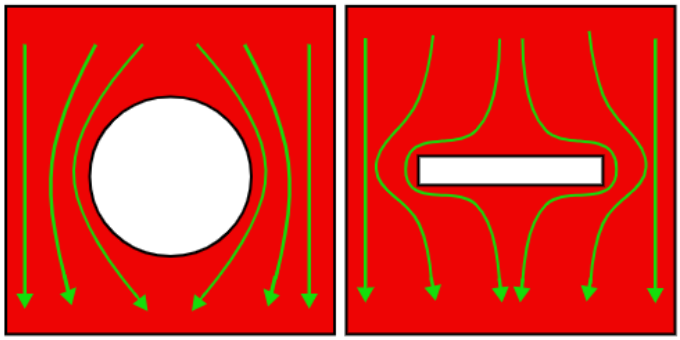

Figure 63 Induced currents: circular and rectangular openings

Analysis of the simulations:

I. Under 40 MHz the results cannot be compared due to DR limitation.

II. [30 MHz -100 MHz]: As in the case mentioned above, unexpected oscillations appear in the simulation results.

III. Over 100 MHz the simulations executed predicts successfully the measured SE.

6.4 Plates №6, №7 & №8: Material And Diameter Size Effect

This section is going to compare Plate Nº6 to Plates Nº6 and Nº7 to study two different parameters:

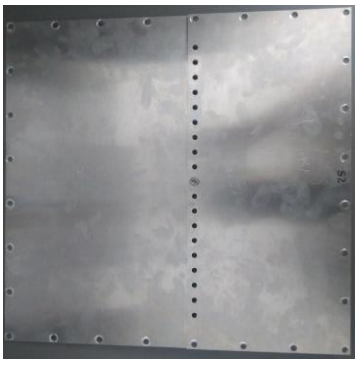

Figure 64 Image of Plate №6 (Front side)

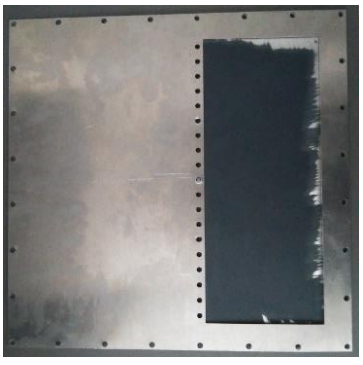

Figure 65 Image of Plate №7 (Back side)

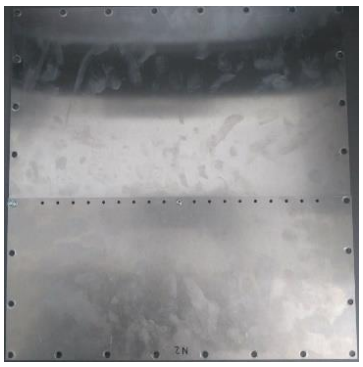

Figure 66 Image of Plate №8 (Front side)

I. Nº6 vs Nº7: The size and shape of both plates is the same. The difference between them is the material the smaller rectangle is made of (Figure 64 and Figure 65).

II. Plate Nº6 vs Nº8: The material, size and number of holes is the same. The only difference is that the diameter of the openings is smaller in Plate Nº8 (Figure 66), 3Ø mm vs 4.5 Ø mm.

The connection between the two sheets that make up the whole plate, as explained in subsection 5.5.2, is assumed to be perfect. Therefore, no resonance is expected in the results.

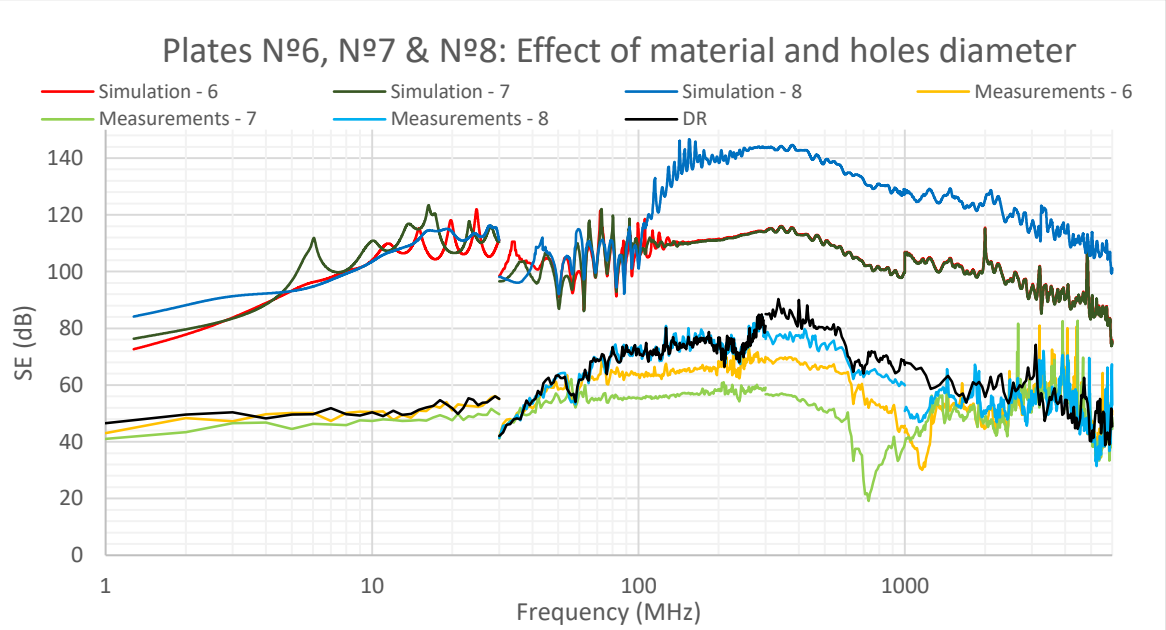

Figure 67 Results of Plates Nº6, Nº7 and Nº8

Analysis of the measurements:

I. The Loop antenna results are invalid, once again, for Plates Nº6 and Nº8. The DR is too close to the measured SE. In the case of Plate Nº7, the SE is slightly below the DR, up to 8 dB at certain frequencies. The accuracy of this values is not very high, but it can be used as a reference close to the real SE of the plate.

II. Results at frequencies higher than 1.3 GHz present the same problem discussed in the previous point, DR limitation. It also affects the measures for the Plate Nº8 under 200 MHz.

III. Each trace presents an important resonance: Plates Nº6 and Nº8 approximately at 1.16 GHz, Plate Nº7 at 730 MHz. The aperture size generating each resonance is:

$$Plates\ Nº6\ and\ Nº8:\ L = \frac{c}{2 \cdot f} \simeq \frac{c}{2 \cdot 1.16\ GHz} \simeq 130\ mm \qquad \textit{Equation 15}$$

$$Plate\ Nº7:\ L = \frac{c}{2 \cdot f} \simeq \frac{c}{2 \cdot 700\ MHz} \simeq 214\ mm \qquad \textit{Equation 16}$$

Although three screws were used (Figure 68) to join both sheets the leakage through the connections is too high. The initial assumption of having a perfect union is invalid. Study of the resonances detected:

- Plates Nº6 and Nº8: The border of the small rectangle sheet is not fully connected to the plate because the screws offer a good electrical connection only in its close-up range. As a consequence, two thin resonant apertures appear between the screw in the middle and the ones at the edges (Figure 68). The length of this apertures cannot be accurately estimated because depends on the area properly connected by the screws, but it must be a value slightly lower than 149.5 mm. This is in line with the size estimated in Equation 15, 130 mm.

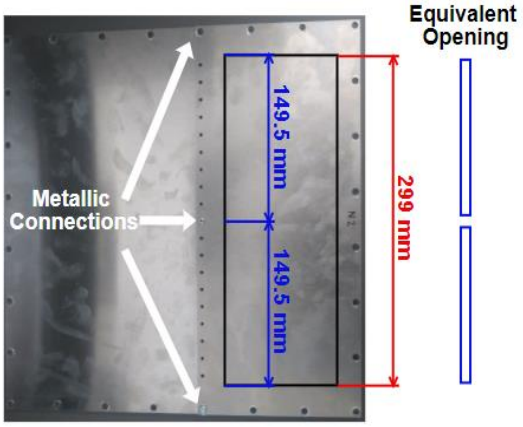

Figure 68 Visual analysis of the imperfections in Plates Nº6, Nº7 and Nº8

- Plate Nº7: Same justification explained for the previous case is applicable to this one. However, the frequency is not the same. It is caused by the layer of "dark blue paint" (Figure 65) with unknown properties covering the rectangular sheet. For Plates Nº6 and Nº8 the dielectric between the pieces was air, but for Plate Nº8 another dielectric, the "paint" is present, with an unknown relative permittivity. It means that the previously calculated 214 mm aperture size for this plate is not correct. On the other hand, the size should be equal to 130 mm, as the structure is practically the same. Making this assumption, the relative permittivity associated to the "paint" can be estimated:

$$\frac{c}{2 \cdot 1.16\ GHz} \simeq 13 \simeq \frac{c}{2 \cdot \sqrt{\epsilon_r} \cdot 730\ MHz} \Rightarrow \epsilon_r = 2.5 \qquad \textit{Equation 17}$$

This value, although reasonable, could not be verified by other methods: comparing to the properties of the sheet (unknown) or measuring the relative permittivity in the laboratory (could not be done). Checking the accuracy of this value is essential to guarantee the correctness of this analysis.

IV. Plate Nº6 vs Nº7: This comparison shows the effect of modifying the sheet material. As expected, if the conductivity of the material is reduced (Plate Nº7) the SE decreases. In the range [60 MHz – 1.2 GHz] the difference is between 10 and 15 dB. Over 1.2 GHz no conclusions can be extracted, the DR is restricting the measurements.

V. Plate Nº6 vs Nº8: In the frequency range with valid results, [300 MHz – 1.2 GHz], the SE improvement achieved by reducing the diameter size from 4.5 mm to 3 mm reaches up to 14 dB.

Analysing the simulations results in this section is unnecessary. The imperfections in the connections mentioned above have a huge impact in the SE. The simulations did not take it into account and overestimate the SE of the plates. Besides, the models could not be redesigned because the width of the aperture is too small and cannot be modelled without increasing excessively the number of voxels/simulation time.

Next subsection uses equivalent plates, but with wider openings, to study the effect of this apertures under different conditions.

6.5 Plate Nº9: Aperture Width And EM Clamps Effect

The plate (Figure 70) was placed with its opening perpendicular to the electric field in order to maximize the power transmitted. The influence of three modifications is going to be analysed in this section: varying the aperture width, placing EM clamps in the middle of the aperture and using bigger clamps.

First analysis is focused on the SE dependency with the aperture width (Figure 69), without using any EM clamp.

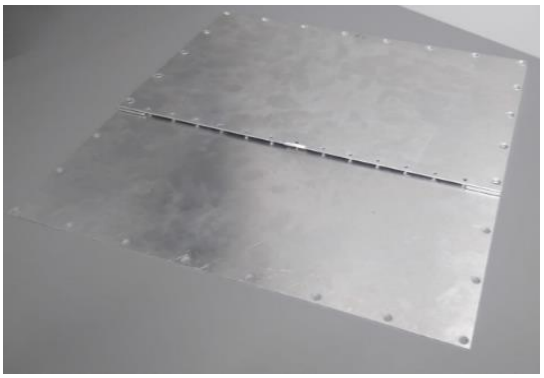

Figure 70 Image of plate Nº9 with a EM clamp in the middle of the opening

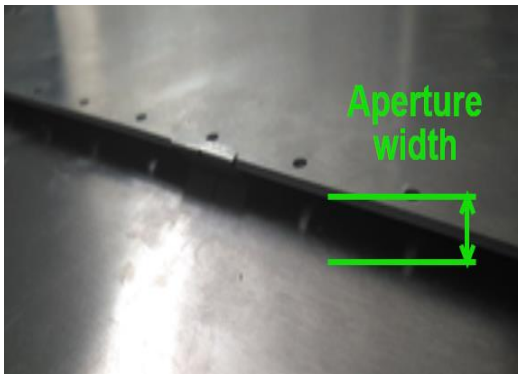

Figure 69 Aperture width of Plate Nº9

First estimated resonant frequency for this configuration:

$$f = \frac{c}{2 \cdot L} \simeq \frac{c}{2 \cdot 299\ mm} \simeq 501\ MHz \qquad \text{Equation 18}$$

Figure 71 shows the results when the width parameter is set to 1 and 5 mm:

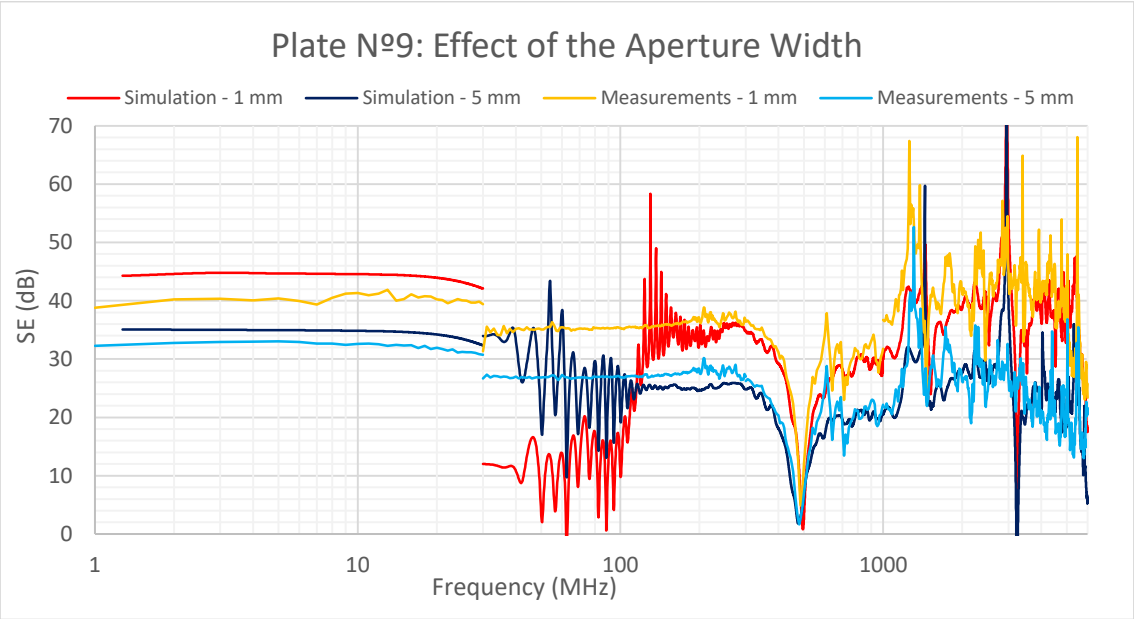

Figure 71 Results of Plate Nº9: No EM clamp and opening width set to 1 and 5 mm

In this section none of the graphs includes the DR because all the measures are under this limit.

Analysis of the measures:

I. The first resonance, that reduces drastically the SE to 0 dB, is located at 500 MHz (the predicted value).

II. Modify the width from 1 to 5 mm has an impact of approximately 7.5 dB in the SE that is independent of the frequency.

Analysis of the simulations:

I. Loop antenna simulation overestimate the SE in both cases: 4.5 dB (1mm) and 2.3 dB (5 mm).

II. [30 MHz -200 MHz]: As in previous simulations, the results in this range are not reliable.

III. From 200 MHz to 1.3 GHz the simulation values fit the measures with high accuracy

IV. Although at frequencies higher than 1.3 GHz (where the wavelength becomes comparable to the set-up dimensions) the fast oscillations in the measures are not so well predicted, the average SE matches.

V. There is a spike in the simulations at 3.2 GHz that has values under 0 dB. This sharp variation is a common malfunction in the calculations that can be ignored. Subsequent simulations will present the same error.

The next factor under analysis is the use of EM clamps. First approach to model this metallic structures assumes its electromagnetic behaviour equivalent to a PEC that stablish an electrical connection between both sheets of the plate (Figure 72).

Figure 72 Model of Plate Nº9 with an EM clamp in the middle of the aperture

Consequently, instead of having one aperture of 299 mm length, there are now two openings of approximately 140 mm. It directly implies doubling the value of the first resonant frequency, that should be close to 1 GHz.

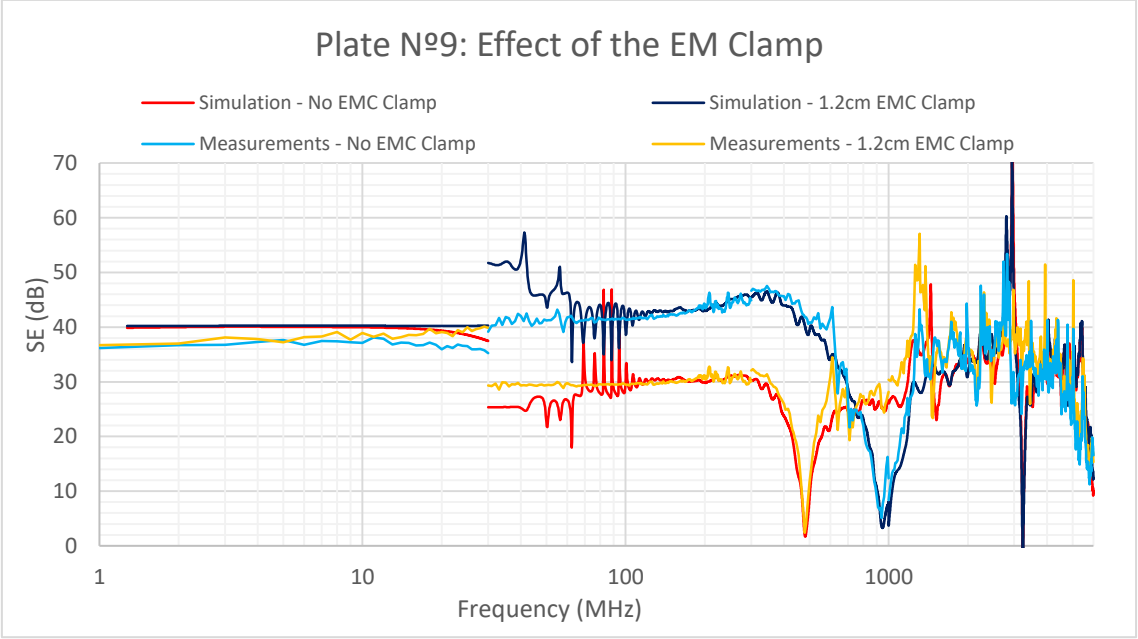

Figure 73 Results of Plate Nº9: EM clamp of 1.2 cm length and opening width set to 2 mm

Analysis of the measurements:

I. In the Loop antenna measurements, the clamp has no impact over the SE. It is because for the magnetic field the most important factor is the area of the aperture, and the clamp does not modify it significantly.

II. From 30 MHz to 1 GHz the offset consequence of the clamp is close to 10 dB. At high frequencies this impact tends to zero.

III. At 1 GHz the plate with the EM clamp presents the expected resonances, which means that the clamp offers a good electrical connection.

Analysis of the simulations:

I. Same issues as in previous cases appear in these results. SE spike at 3.2 GHz and mismatch in the range [30 MHz -100 MHz].

II. Apart from the previous issues the simulations fit the measurements with high precision.

The last parameter under study is the length of the EM clamp:

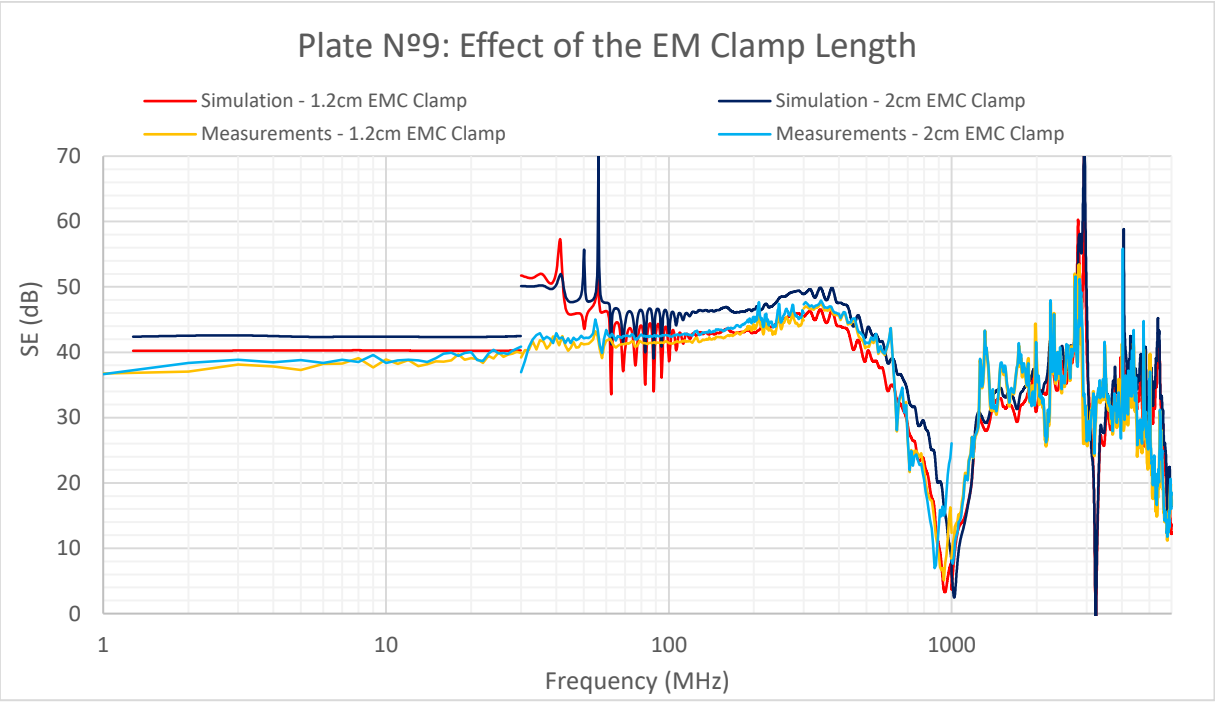

Figure 74 Results of Plate Nº9: EM clamps of 1.2/2 cm length and opening width set to 2 mm

Figure 74 proves that modifying the length has no impact on the measurements, whose difference is practically null. On the other hand, in the simulations, a higher EM clamp length has an impact under 1 GHz of approximately 6 dB.

Consequently, the best approach for both clamps is the model with a length of 1.2 cm, that fits with high precision the measurements.

6.6 Plate Nº10: Net Modelling

Designing this plate was complex due to the several holes drilled in the net, despite its impact is practically null compared to the rectangular opening.

Setting the net thickness in the model was an extra issue. It is very problematic modelling dimensions smaller than 1mm because of the excessive increase in the simulation time. Two solutions were possible, assume 1 mm thickness or null. Both designs were made and simulated to evaluate its correspondence with the measurements.

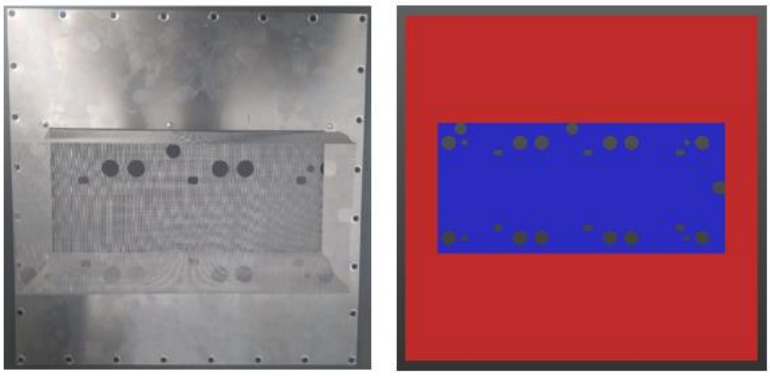

Figure 75 Plate Nº10: Original (Left) and Model (Right)

Once the design was ready, defining the net material properties was the next challenge. As no information about its electrical conductivity was provided, the first approach was presuming a high value. Therefore, the 1mm thickness design was associated to PEC properties and the other one to TRS with σ_c= 1000000 S/m (which is in practice equivalent to a PEC).

The impact of each definition in the number of cells used to simulate the scenario is shown in Table 12:

	Antenna		
Material	Loop	Bilog	Horn
TRS	66.019	172.571	42.482
PEC	69.021	204.421	45.274

Table 12 Nº of Mcells required for the simulation

As expected, the number of cells is lower for the TRS option because no voxels must be defined for the net. It directly reduces the simulation time.

Figure 76 plots the values obtained for each simulation:

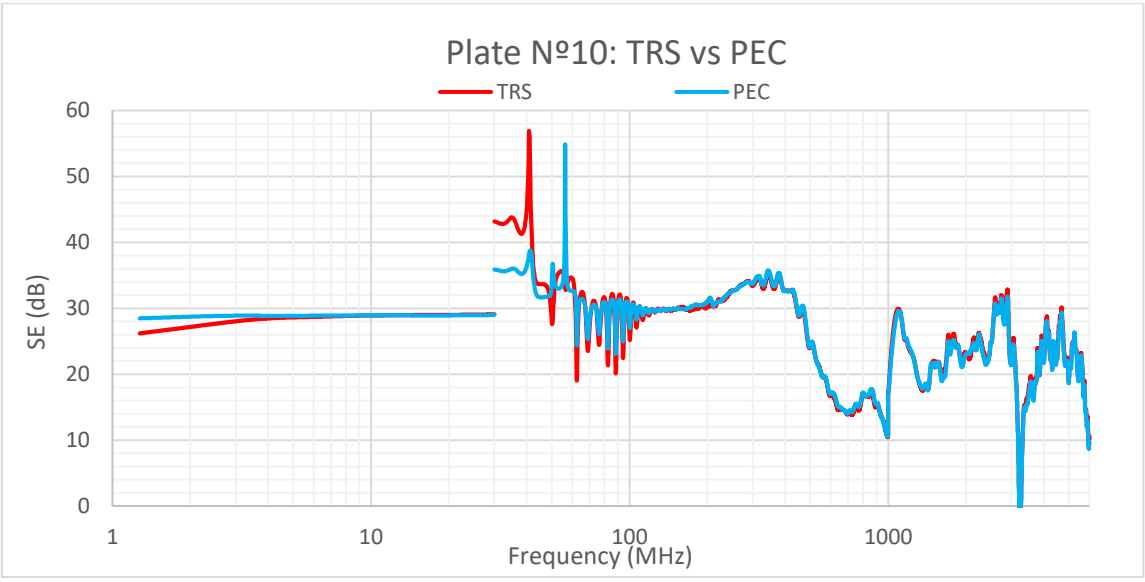

Figure 76 Simulations of Plate Nº10

The difference between both options is negligible except for the frequency range [30 MHz – 100 MHz]. However, as explained before, the simulation does not work properly at these frequencies and the values are not reliable. A solution for this is offered at the end of this chapter.

As the results are equivalent the TRS option is the one chosen for two reasons:

I. Lower number of cells, faster simulations.

II. TRS offers the option of selecting the electrical conductivity, which could be necessary.

Next graph, Figure 77, compares the TRS simulation to the measurements:

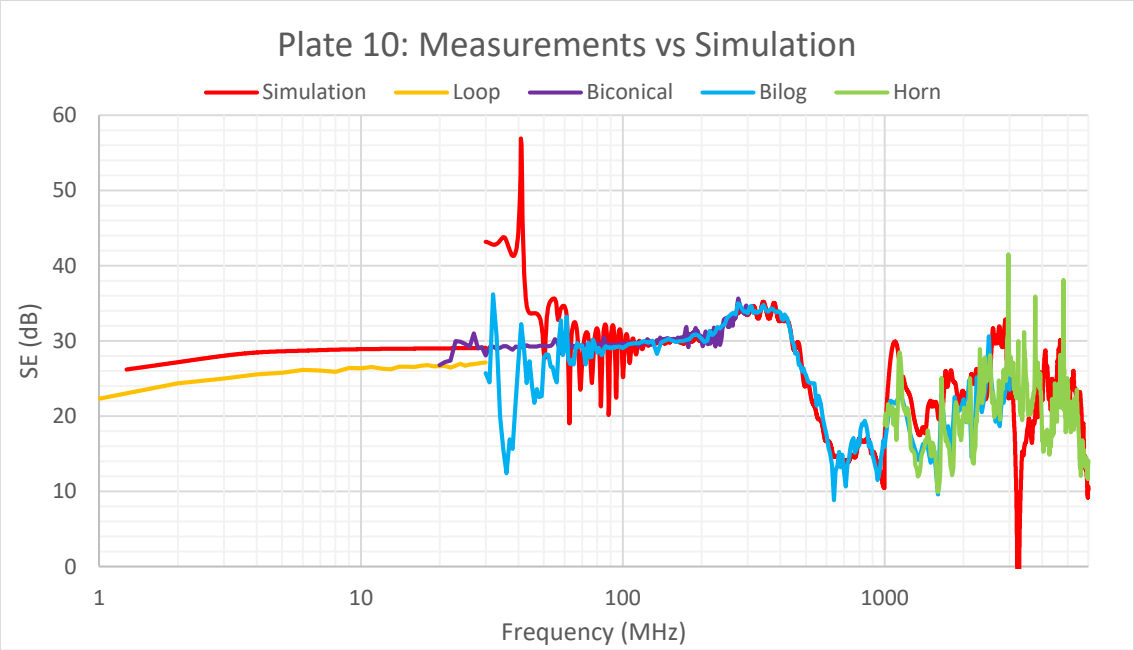

Figure 77 Results of Plate Nº10

Figure 77, in contrast to previous graphs, shows all the measures taken with the Bilog antenna because does not block the vision of the other results.

Analysing the SE measurements and trying to associate its evolution to certain physical characteristics of the plate is not affordable in this case, the structure is too complex.

Furthermore, the objective of studying this plate is to find out if the simulation can predict suitably the measurements:

I. Simulation for the loop antenna overestimate by 5 dB the SE, which is within the acceptable range.

II. The accuracy of the Bilog antenna is quite high in all the range except for the well-known issue between 30 MHz and 100 MHz.

III. At 3.27 GHz the simulation results decay drastically under 0 dB, as in the previous section. Except for this deviation, over 1 GHz the simulation predicts successfully the measurements.

6.7 Mismatch Between Simulations And Measurements

The simulations results in the frequency range [30 MHz – 200 MHz] have presented a very poor accuracy for several plates. First approach to solve this issue was increasing the number of periods simulated. However, it increased the computing time without solving the problem.

The second approach was reducing the simulation broadband from [30 MHz – 1 GHz] to [30 MHz – 200 MHz]. This modification, as Figure 78 displays, fixed the mismatch.

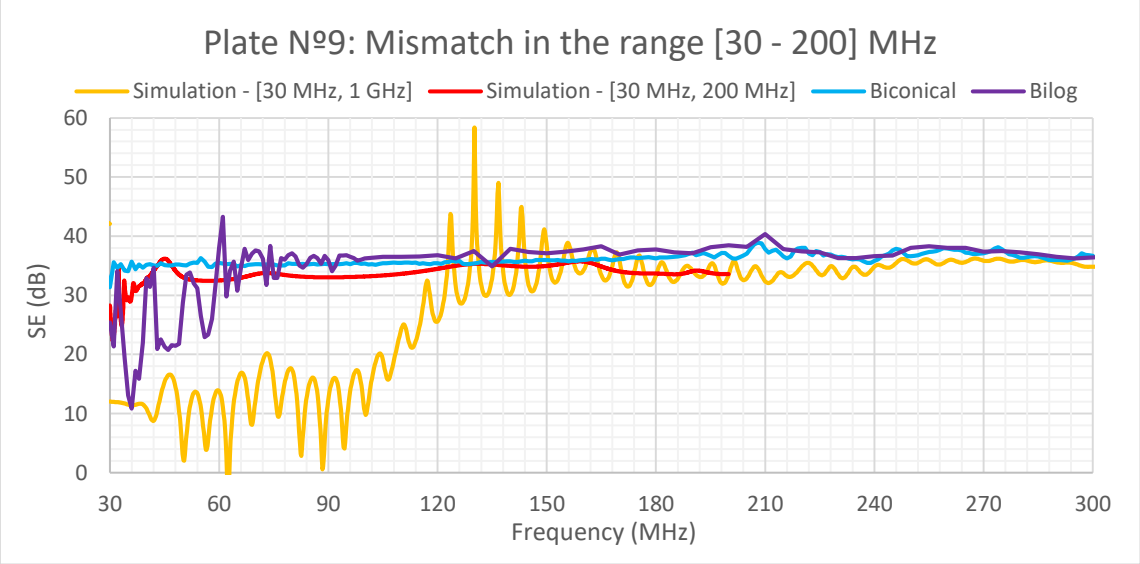

Figure 78 Results of Plate Nº9: No EM clamp and opening width set to 5 mm

The highest frequency initially simulated (1 GHz) was 33 times the lowest one (30 MHz), this is the origin of the measurements-simulations divergence. The gaussian sine pulse generated by the source decreases its accuracy for the lower frequencies. When the bandwidth is reduced the simulation fits perfectly the measurementss and the oscillations disappear.

Chapter 7

Conclusions and Future Research Lines

The learning outcomes of the investigation are summarized in this final chapter and analysed from a critical point of view. In addition, future research lines are proposed in order to continue improving the system.

7.1 Conclusions

This research work started using as knowledge base a precedent investigation developed in Seibersdorf Laboratories. That project had proposed a SE determination method in the anechoic chamber with the Bilog and Horn antennas. The proposal feasibility was evaluated with a couple of simple openings. The set-up was also simulated proving a good estimation of the measures from 200 MHz to 6 GHz, but not in the range [30 MHz – 200 MHz].

On this basis, the investigation pretended to:

I. Increase the bandwidth under analysis by adding the frequency range [1 MHz – 30 MHz].

II. Find the set-up configuration that offers the highest SE measurable.

III. Measure the SE of openings with different characteristics: shape, size, material, EM clamp.

IV. Model appropriately the plates to develop accurate simulations.

V. Fix the simulations results in the frequency range [30 MHz – 200 MHz].

First objective, increasing the bandwidth: It required a theoretical investigation. Standard IEEE 299 proposes using Loop antennas in these frequencies because experience has proved that the most stringent requirement is the magnetic-field shielding. This recommendation was followed, Loop antennas were used to evaluate the SE from 1 MHz to 30 MHz.

Second objective, find the best set-up configuration: two modifications were considered: using different types of antennas and varying the antenna-wall distance. Apart from the Bilog and Horn antennas used in the original project and the mentioned Loop antenna, the Biconical and LPDA antennas were also tested. About the distance parameter, three different values were measured. The results proved that:

I. The antenna used does not modify the SE measured. It could be seen in the overlapped frequencies: [30 MHz – 200 MHz] Biconical/Bilog, [200 MHz – 3 GHz] Bilog/LPDA, [1 GHz – 3 GHz] Bilog/Horn.

II. DR of the Bilog antenna from 30 MHz to 200 MHz is very low, the Biconical antenna performance is better and must be used in this range.

III. LPDA performance is equivalent to the Bilog Antenna, same DR.

IV. DR decreases as distances increases under 200 MHz. Over 200 MHz the DR is independent of this factor.

V. SE is independent of the distance under 1 GHz. For higher frequencies having the antenna too close can interfere in the measurements.

Optimal configuration according to the previous results. The optimal DR is over 40 dB for the whole analysed bandwidth:

Antenna Type	**Bandwidth Analysed**	**Distance Antenna – Wall**
Loop	1 MHz – 30 MHz	30 cm
Biconical	30 MHz – 200 MHz	100 cm
Bilog	200 MHz – 3 GHz	50 cm
Horn	1 GHz – 6 GHz	55 cm

Table 13 Configuration of the set-up that maximize the DR

Third objective, measuring the SE of the 10 plates: The following dependencies between the electromagnetic attenuation offered by the plate and its opening characteristics were demonstrated:

- Plates Nº1 & Nº3: Rounding the corners of a rectangular slot does not significantly affect the SE.
- Plate Nº2: The orientation of the opening is of paramount importance if the aperture height is bigger/smaller than the width.
- Plate Nº2: The first resonant frequency for rectangular slots can be estimated with high precision using Equation 19 ("L" equal to the maximum size of the aperture in the dimension perpendicular to the electric field)

$$f = \frac{c}{2 \cdot L} \qquad \textit{Equation 19}$$

- Plates Nº4 & Nº5: Equation 19 is not applicable to circular openings. There are no relevant resonances in these structures for linearly polarized waves.
- Plates Nº4 & Nº5: The effect of the diameter size over the SE decreases with the frequency, becoming negligible over 2.7 GHz.
- Plates Nº6, Nº7 & Nº8: It cannot be assumed that joining metallic sheets using a screw is equivalent to a perfect electrical connection. The leakage is too important through the borders.

- Plate Nº7: Metallic sheets made of a less conductive material offer lower SE.
- Plate Nº9: The width of the aperture has a direct impact on the SE. Setting it to 1 mm instead of 5 mm increase the SE in 10 dB.
- Plate Nº9: Set an EM clamp in the middle of the opening stablish a good electrical connection that increase the SE for the low frequencies and doubles the frequency at which appears the first resonance.
- Plate Nº9: The length of the EM clamp does not have an important impact in the SE.

Fourth objective, model the plates:

- Plates Nº1-5: Plates with simple openings. The metallic sheet was assumed to have PEC properties. Simulations estimate with high accuracy the measurements.
- Plates Nº6-8: The model of these plates was inappropriate. The leakage through the connections between the sheets was too high and, therefore, the SE was overestimated in the simulations.
- Plate Nº9: Simplifying the EM clamps by modelling it as rectangular cuboids with PEC properties proved being a good approximation for the simulations
- Plate Nº10: Net can be modelled as a PEC or a TRS with high conductivity. Both options predict properly the measured SE. However, the TRS reduces the simulation time because it requires less voxels.

Fifth objective, fixing the simulations inaccuracies from 30 MHz to 200 MHz: Solving this issue was quite simple and just required reducing the broadband used in simulation. An excessive ratio between the highest and the lowest simulated frequency decreases the accuracy in the lower part of the band.

Accomplishing these objectives has been useful to improve the SE determination method in two different ways:

- Measurements: The broadband measured has been increased by adding the frequency range [1 MHz – 30 MHz]. Studying the impact of using other antennas and distances has led to an improvement on the DR.
- Simulations: The simulated broadband has been increased to cover the new measured range with successful results. There is as well a better knowledge on how to model EM clamps and nets.

7.2 Future Research Lines

This investigation has proved good results dealing with thin drilled metallic sheets with properties equivalent to PEC. Upcoming projects should study in depth the impact of using other materials or thicker plates. Applying new materials would drastically increase the complexity of the scenario because an accurate knowledge of the material electromagnetic properties and its dependence with the frequency would be necessary.

It must be also considered that the measuring methodology has been developed to study the openings impact on the SE. In case of working with solid blocks our approach may not be the best solution. As it can be seen in Annex B, applying this set-up to solid stones leads to conflicting results. For these new conditions an alternative methodology has been proposed. Further research should continue working on improving the measuring in the laboratory and developing accurate simulations.

Another line of investigation could be the analysis of PCBs, this way the application range of the simulations would be increased. Successful simulations of simple circuits would be a first step to more complex scenarios. Two possible approaches: identify and simulate only the current paths that are generating the radiations or use suitable models provided by the manufacturers.

Annex A: Dimensions of the Plates Apertures

Plate	Aperture Dimensions (mm)
1	24x43
2	24x117
3	25x41
4	40Ø
5	55Ø
6	Main sheet opening: 121x299; Small rectangle: 157x344; Holes: 4.5Ø
7	Main sheet opening: 121x299; Small rectangle: 157x344; Holes: 4.5Ø
8	Main sheet opening: 121x299; Small rectangle: 157x344; Holes: 3Ø
9	Main sheet opening: 180x299; Small rectangle: 215x344
10	Net: 130x280x85

Table 14 Apertures dimensions

Annex B: Stones Measurements

The SE of three stones made of the same material and with different thicknesses (5, 10 and 15 cm) was measured at a customer´s request. The electromagnetic properties of the stones were not provided by the manufacturer.

Semi-Anechoic Chamber

The stones were measured from 100 MHz to 18 GHz and fixed to the square opening using a metallic frame clamped with metallic bolts and nuts (Figure 79).

Figure 79 Set-up for the SE determination of the stones in the semi-anechoic chamber

Results for each stone with Figure 79 configuration:

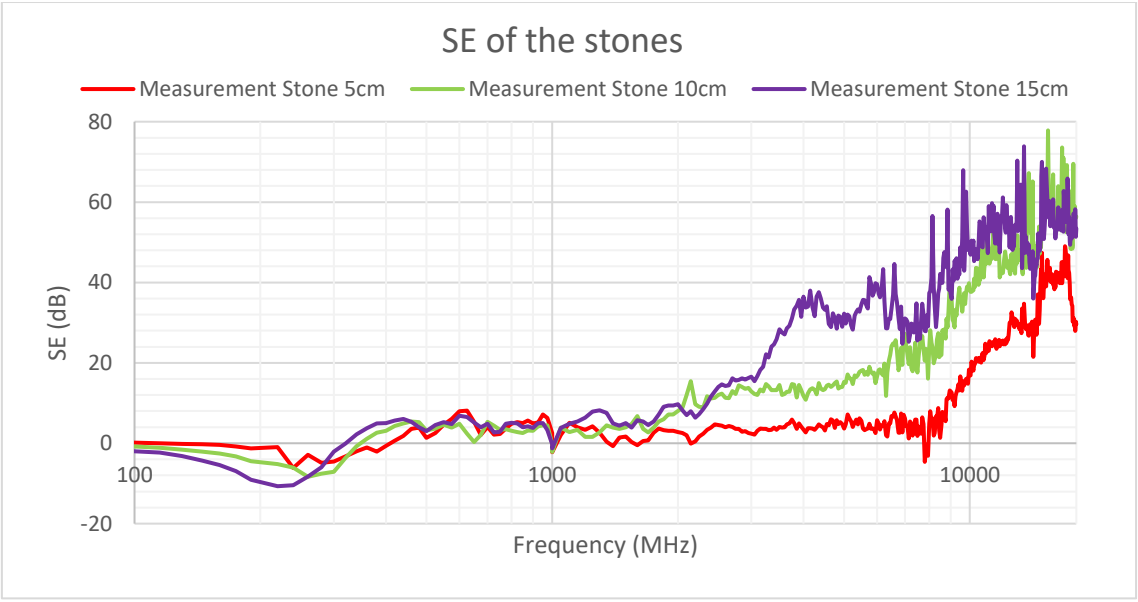

Figure 80 Results of the stones in the semi-anechoic chamber

The results obtained were not the expected ones. From 100 MHz to 300 MHz we had a negative SE for all the stones and at 8 GHz for the 5 cm thick stone. This raised the suspicion that some undesired effects were affecting the measurements and we were not determining the real SE. The first proposal was changing the metallic frame, bots and nuts (Figure 81) by others made of plastic (Figure 82) (invisible to the electromagnetic fields).

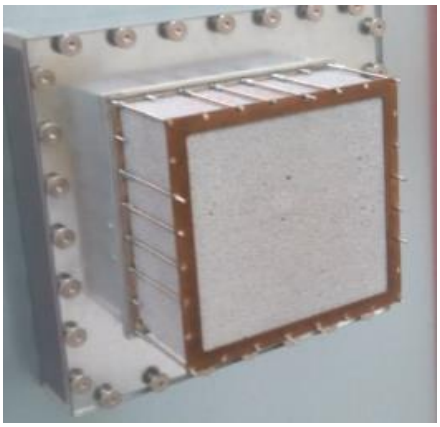

Figure 81 Metal fixing

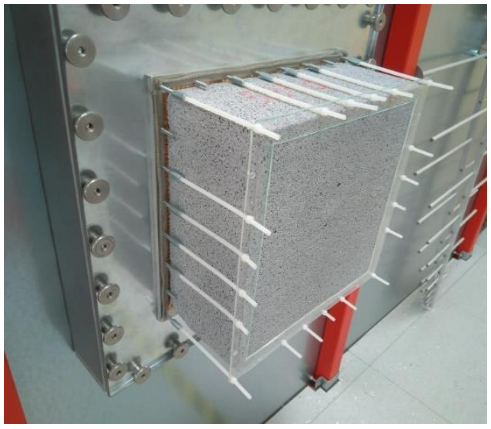

Figure 82 Plastic fixing

However, this modification did not change the measured SE.

Another origin of the undesired results could be the diffraction on the stone borders, it may be entering into the chamber. Nevertheless, the stone side facing the transmitter antenna could not be set in line with the aperture frame due to its design limitations.

At this point we had reached an impasse and no explanation for the unexpected results was found. The solution to the problem was using a different set-up to determine the SE.

Fully-Anechoic Chamber

This subsection presents the measurements of the stones in the fully-anechoic chamber. The SE is defined as the difference between the power received with the free-space configuration (Figure 83) and with the stone between the antennas (Figure 84).

Figure 83 Set-up with free-space conditions in the fully-anechoic chamber

Figure 84 Set-up with the stone between the antennas in the fully-anechoic chamber

These measurements can only be done with the Horn antennas due to the small size of the stones, with other devices the leakage through the borders would be too important. Even with the Horn antennas, an excessive distance between transmitter and receiver could produce leakage. Therefore, the SE was measured for different distances (considering as reference the front side of the antennas).

It is assumed that the material used to hold the stones is electromagnetically invisible.

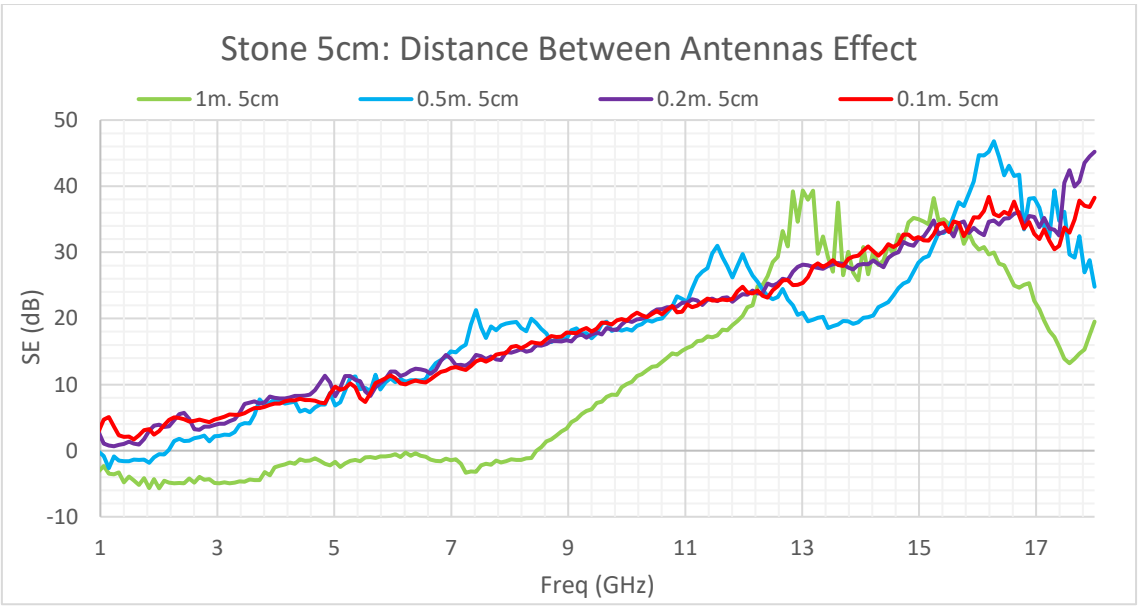

Figure 85 Results of the 5 cm thick stone in the fully-anechoic chamber

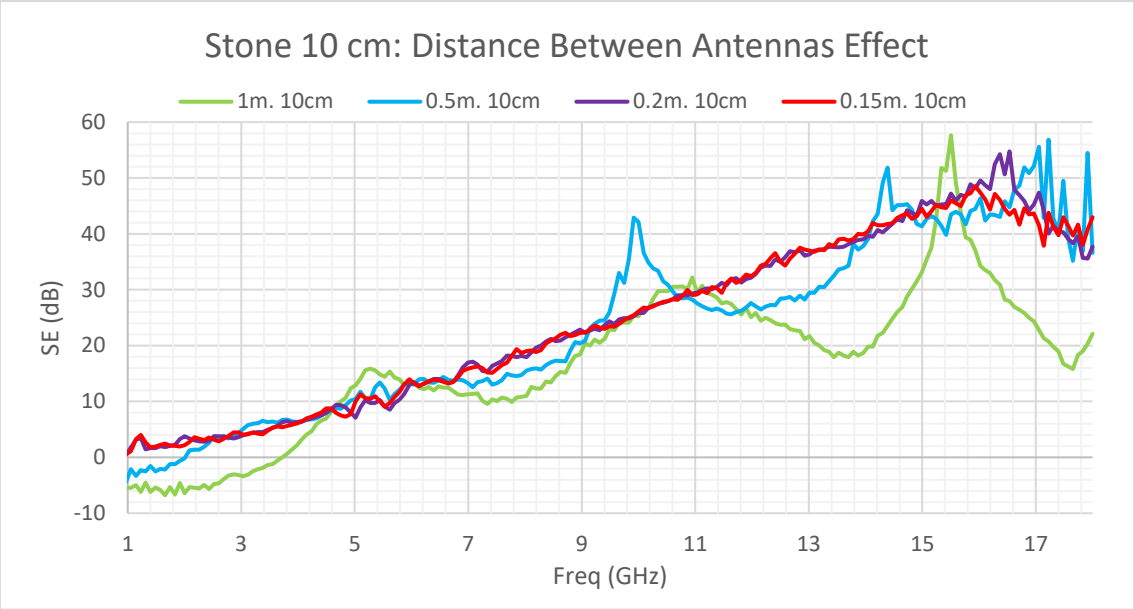

Figure 86 Results of the 10 cm thick stone in the fully-anechoic chamber

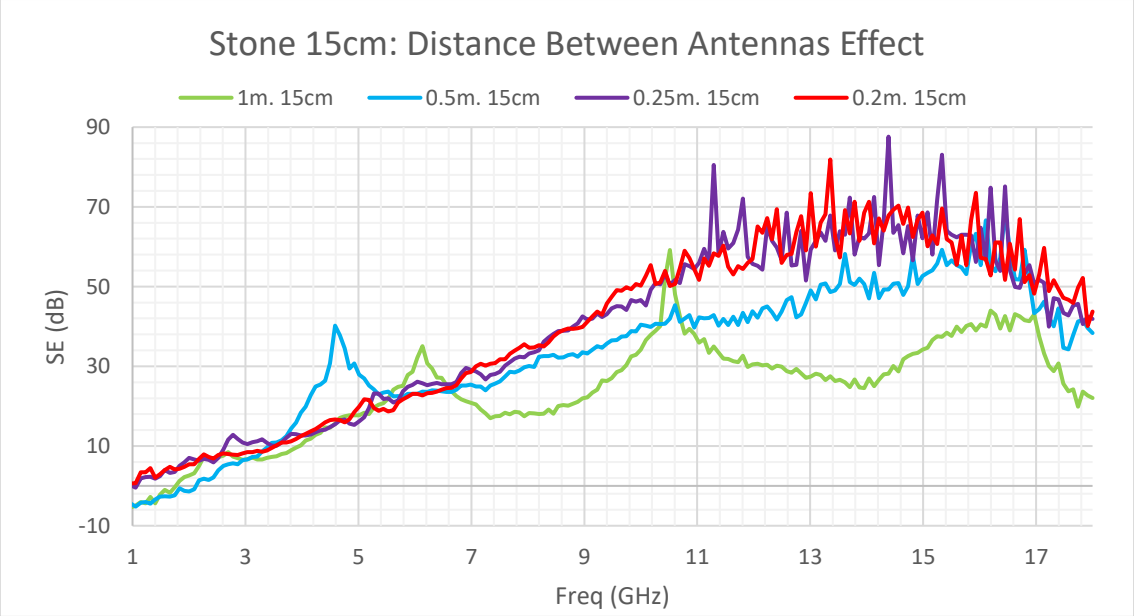

Figure 87 Results of the 15 cm thick stone in the fully-anechoic chamber

In the three cases the SE becomes independent of the distance for values lower than 25 cm. It implies that the leakage through the borders becomes negligible. Figure 88 compares the results of each stone when the distance is set to 20 cm:

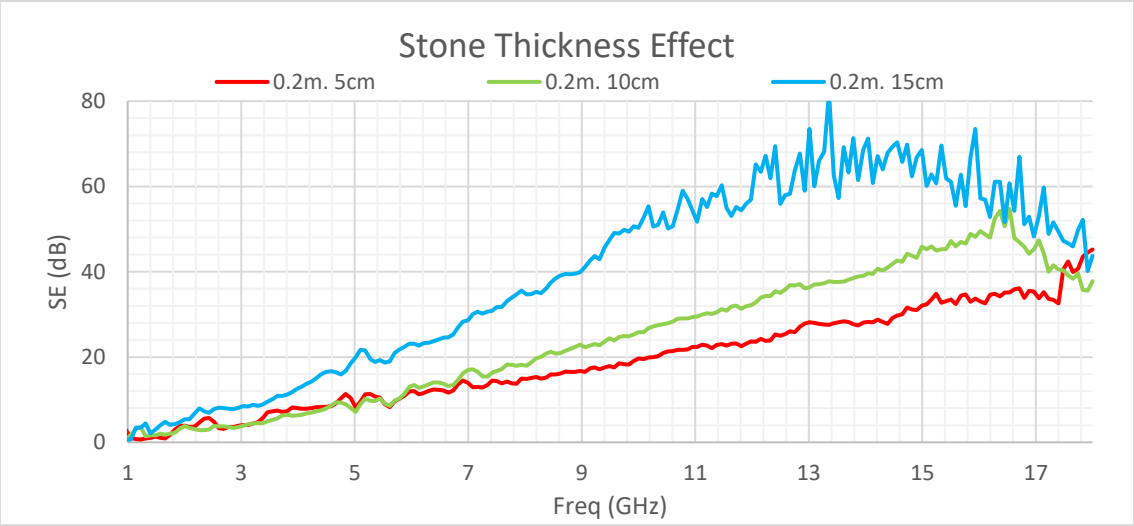

Figure 88 Results of the stones with the distances between antennas set to 20 cm in the fully-anechoic chamber

The obtained SE values are more in line with the expected results. This set-up seems to be more appropriate to measure structures without openings.

Annex C: Net Measurements

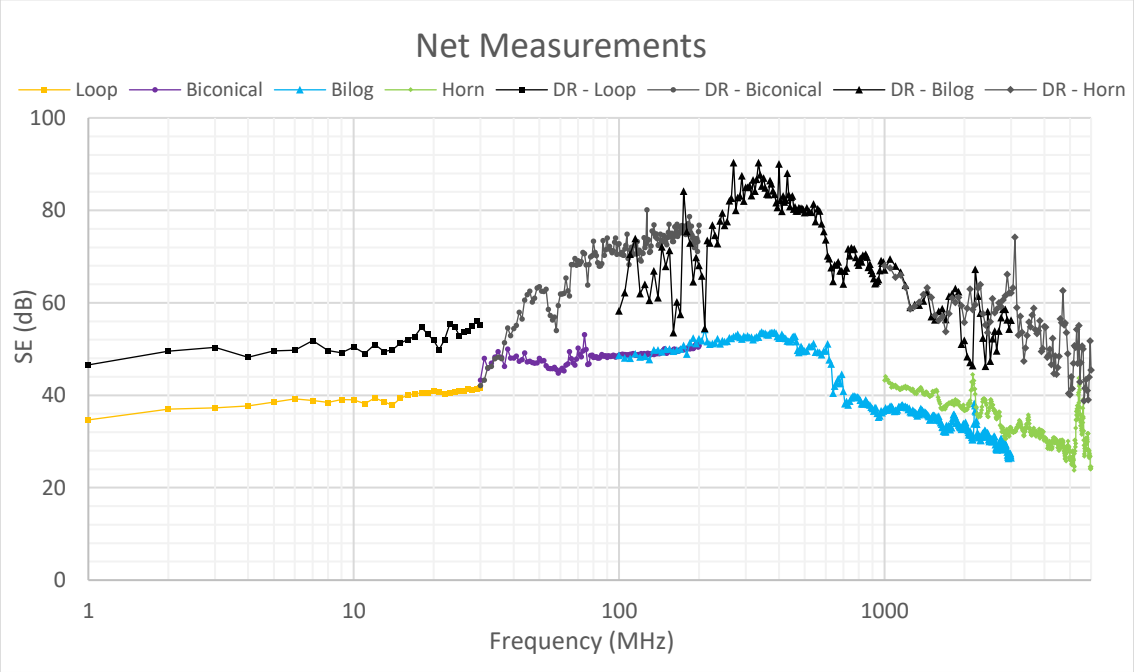

Figure 89 Net Measurements

In Figure 89 the measures for Bilog and Horn antenna do not overlap. The reason is that when the net was placed in the square opening it was not possible to fix it flat, it was slightly wavy. Between measurements with both antennas the net had to be taken off and put back on. At these frequencies the wavelength is comparable to the net dimensions and the unavoidable slight changes on its shape affected directly to the measured SE.

Bibliography

[1] Seibersdorf Laboratories. “Behind the new brand lies and accomplished team!” (Online). Available: *https://www.seibersdorf-laboratories.at/en/company-info/about-us* (Accessed: 09 - July - 2018).

[2] Henry W. Ott. “Electromagnetic Compatibility Engineering”. John Wiley & Sons, 2009.

[3] Magnus Karlsson. “EMC and PCB design: Lecture 1”. Course: Electromagnetic Compatibility and Printed Circuit Board Design, Linköping University, 2015.

[4] Standards Development Committee of the IEEE Electromagnetic Compatibility Society. “IEEE Std. 299-2006”, “IEEE Standard Method for Measuring the Effectiveness of Electromagnetic Shielding Enclosures”, 2006.

[5] C. L. Holloway, J. Ladburry, J. Coder, G. Koepke and D. A. Hill. “Measuring Shielding Effectiveness of Small Enclosures/Cavities with a reverberation chamber”. IEEE International Symposium on Electromagnetic Compatibility, pp. 1-5.

[6] Jan Carlsson, Kristian Karlsson and Andreas Johansson. “Validation of Shielding Effectiveness Measurement Method Using Nested Reverberation Chambers by Comparison with Aperture Theory”. SP Technical Research Institute of Sweden and Lund University.

[7] M. Hromádka and Z. Kubík. “Suggestion for Changes in Shielding Effectiveness Measuring Standard”. Department of Applied Electronics and Telecommunications, University of West Bohemia.

[8] Z. Kubík and J. Skála. “Shielding Effectiveness Measurement and Simulation of Small Perforated Shielding Enclosure Using FEM”. Department of Applied Electronics and Telecommunications, University of West Bohemia.

[9] Surendra Loya and Habibullakhan. “Analysis of Shielding Effectiveness in the Electric Field and Magnetic Field and Plane Wave for Infinite Sheet Metals”. International Journal of Electromagnetics and Applications, 2016, 6(2):31-41.

[10] C. R. Paul. “Introduction to Electromagnetic Compatibility”, 2nd edition. Wiley Series in Microwave and Optical Engineering, 2006.

[11] Rohde-Schwarz. “R&S®SMB100A RF and Microwave Signal Generator” (Online). Available: *https://www.rohde-schwarz.com/es/producto/smb100a-pagina-de-inicio-producto_63493-9379.html* (Accessed: 25 - October - 2018).

[12] Rohde-Schwarz. “R&S®ESW EMI Test Receiver” (Online). Available: *https://www.rohde-schwarz.com/es/producto/esw-pagina-de-inicio-producto_63493-121280.html* (Accessed: 25 - October - 2018).

[13] Teseq GmbH. “HLA 6121: 60 cm Loop Antenna 9 kHz to 30 MHz” (Online). Available: *http://www.teseq.com/products/HLA-6121.php* (Accessed: 10 - July - 2018).

[14] Teseq GmbH. “VBA 6106: Biconical Antenna 30 MHz – 300 MHz” (Online). Available: *http://www.teseq.com/products/VBA-6106.php* (Accessed: 10 - July - 2018).

[15] Teseq GmbH. “UPA 6109: Log Periodic Antennas 200 MHz to 1 GHz” (Online). Available: *http://www.teseq.com/products/UPA-6109.php* (Accessed: 10 - July - 2018).

[16] Teseq GmbH. “CBL 6111: BiLog Antenna 30 MHz to 1 GHz” (Online). Available: *http://www.teseq.com/products/CBL-6111.php* (Accessed: 10 - July - 2018).

[17] Teseq GmbH. “CBL 6143: Compact X-Wing Bilog Antenna 30 MHz to 3 GHz” (Online). Available: *http://www.teseq.com/products/CBL-6143.php* (Accessed: 10 - July - 2018).

[18] Teseq GmbH. “BHA 9118: Broadband Horn Antenna 1 to 18 GHz” (Online). Available: *http://www.teseq.com/products/BHA-9118.php* (Accessed: 10 - July - 2018).

[19] SPEAG. “SEMCAD X Matterhorn SOLUTIONS” (Online). Available: *https://www.speag.com/products/semcad/solutions* (Accessed: 16 - July - 2018).

[20] Schmid & Partner Engineering AG. “SEMCAD X Reference Guide”. November 2013, p. 150.

[21] Schmid & Partner Engineering AG. “SEMCAD X Reference Guide”. November 2013, pp. 115-116.

[22] FDTD. “The Space/Time Stability Conditions” (Online). Available: *https://fdtd.wikispaces.com/The%20Space-Time%20Stability%20Conditions* (Accessed: 17 - July - 2018).

[23] Schmid & Partner Engineering AG. “SEMCAD X Reference Guide”. November 2013, pp. 116-117.

[24] Schmid & Partner Engineering AG. “SEMCAD X Reference Guide”. November 2013, pp. 122-123.

[25] Schmid & Partner Engineering AG. “SEMCAD X Reference Guide”. November 2013, p. 131.

[26] Schmid & Partner Engineering AG. “SEMCAD X Reference Guide”. November 2013, pp. 123-124.

[27] Schmid & Partner Engineering AG. “SEMCAD X Reference Guide”. November 2013, pp. 149-151.